

1 **Terrestrial aridity and its response to greenhouse warming**
2 **across CMIP5 climate models**

3 Jacob Scheff* and Dargan M. W. Frierson

4 *Dept. of Atmospheric Sciences, University of Washington, Seattle, Washington*

5 * *Corresponding author address:* Jacob Scheff, Lamont-Doherty Earth Observatory, 301F Oceanog-
6 raphy, 61 Route 9W / PO Box 1000, Palisades, NY 10964.

7 E-mail: jscheff@ldeo.columbia.edu

ABSTRACT

8 The aridity of a terrestrial climate is often quantified using the dimensionless
9 ratio P/PET of annual precipitation (P) to annual potential evapotranspiration
10 (PET). In this study, the climatological patterns and greenhouse warming re-
11 sponses of terrestrial P , Penman-Monteith PET , and P/PET are compared
12 among 16 modern global climate models. The large-scale climatological val-
13 ues and implied biome types often disagree widely among models, with large
14 systematic differences from observational estimates. In addition, the PET
15 climatologies often differ by several tens of percent when computed using
16 monthly versus 3-hourly inputs.

17 With greenhouse warming, land P does not systematically increase or de-
18 crease, except at high latitudes. Therefore, due to moderate, ubiquitous PET
19 increases, P/PET decreases (drying) are much more widespread than in-
20 creases (wetting) in the tropics, subtropics and midlatitudes in most models,
21 confirming and expanding on earlier findings. The PET increases are also
22 somewhat sensitive to the time resolution of the inputs, though not as system-
23 atically as for the PET climatologies.

24 The changes in the balance between P and PET are also quantified using
25 an alternative aridity index, the ratio $P/(P + \text{PET})$, which has a one-to-one
26 but nonlinear correspondence with P/PET . It is argued that the magni-
27 tudes of $P/(P + \text{PET})$ changes are more uniformly relevant than the mag-
28 nitudes of P/PET changes, which tend to be much higher in wetter regions.
29 $P/(P + \text{PET})$ and its changes are also found to be excellent statistical predic-
30 tors of the land-surface evaporative fraction and its changes.

31 1. Introduction

32 Our everyday experience tells us that precipitation (P) is one of the factors that determines the
33 effective wetness or dryness of a terrestrial climate, but not the only one. For example, the “emer-
34 ald city” of Seattle, Washington receives $\sim 950 \text{ mm yr}^{-1}$ of P on average. Yet the environment
35 of Dallas, Texas, which also averages $\sim 950 \text{ mm yr}^{-1}$ of P , seems much drier. This is because its
36 more intense sunshine and warmer, drier air evaporate plant and soil water more effectively.

37 Therefore, when characterizing climatic aridity, it makes sense to consider P relative to potential
38 evapotranspiration PET (e.g. Hartmann 1994), the rate at which the climate demands water from
39 well-watered vegetation. PET is best computed from climate data using the Penman-Monteith
40 equation (section 2), which is just the solution to the physical equations for the energy balance
41 that would hold over a wet surface in given climatic conditions (e.g. Monteith 1981; Allen et al.
42 1998, 2005). According to one standard dataset (Food and Agriculture Organization 2004), PET in
43 Seattle is $\sim 840 \text{ mm yr}^{-1}$, but PET in Dallas is $\sim 1560 \text{ mm yr}^{-1}$, far more water than can actually
44 be supplied by P . Of course, an extensive wet area would cool and moisten those climatic con-
45 ditions, lowering the PET estimates, but plants in a given environment experience its actual (hot,
46 dry) climate, so for ecological purposes it is sensible to use the actual climate when computing
47 PET. The concept of PET is also known as reference evapotranspiration, potential evaporation, or
48 evaporative demand, and is very closely related to pan evaporation.

49 The simplest measure that accounts for the relative magnitudes of P and PET is the ratio of
50 their climatological annual mean values, the aridity index P/PET (e.g. Transeau 1905; Budyko
51 and Miller 1974; Middleton and Thomas 1997; Feng and Fu 2013), which can be thought of
52 as a nondimensionalized precipitation. P/PET indicates whether evapotranspiration should be
53 water-limited ($P \ll \text{PET}$) or energy-limited ($P \gg \text{PET}$), and a difference in P/PET between two

54 climates implies a difference in limiting-factor importance. From the above data, P/PET is ~ 1.13
55 in Seattle, but only ~ 0.61 in Dallas. Budyko and Miller (1974) and earlier workers noted that the
56 same values of P/PET correspond to similar vegetation densities and runoff ratios across widely
57 varying temperature, radiation and PET regimes on Earth. This observation has led to the use of
58 P/PET as the main moisture variable in several prominent terrestrial biome classification schemes
59 (e.g. Middleton and Thomas 1997; Holdridge 1967). In the Middleton and Thomas (1997) scheme,
60 which has been adopted by the United Nations (e.g. Mortimore 2009), $P/PET < 0.05$ is defined
61 as hyperarid, $0.05 < P/PET < 0.2$ as arid, $0.2 < P/PET < 0.5$ as semiarid, $0.5 < P/PET < 0.65$
62 as dry subhumid, and $P/PET > 0.65$ as humid. The climate of Dallas is thus dry subhumid while
63 that of Seattle is quite humid, even though P is the same.

64 Global climate models (GCMs) are often used to generate hydroclimatic responses to various
65 forcings. However, these responses have usually been characterized in terms of individual dimen-
66 sional quantities such as P , actual evapotranspiration (E or ET), runoff, and/or soil moisture (e.g.
67 Collins et al. 2013; Meehl et al. 2007), or in terms of complicated metrics of local drought relative
68 to some reference period, such as the Palmer Drought Severity Index or PDSI (Cook et al. 2014;
69 Dai 2013). The characterization of the models' mean states has been similarly concerned with
70 individual variables, and has often focused on features over the oceans, especially for P (e.g. Flato
71 et al. 2013). In contrast, very few studies have tried to quantify the patterns of general land aridity
72 in climate models, or of the response of aridity to forcing. Here we propose to build on the work of
73 Feng and Fu (2013) by mapping P/PET , its response to greenhouse warming, and its contributing
74 factors across a wide range of modern GCMs over global land.

75 2. Methods

76 Given values of near-surface air temperature T_a , water-vapor pressure e_a , windspeed $|u|$, and net
 77 downward broadband radiation R_n , the Penman-Monteith equation for PET is:

$$\text{PET} = \left(\frac{\Delta(R_n - G) + \rho_a c_p (e^* - e_a) C_H |u|}{\Delta + \gamma(1 + r_s C_H |u|)} \right) / L_v, \quad (1)$$

78 where e^* is the saturation vapor pressure at T_a , $\Delta := de^*/dT(T_a)$ is a standard notation for the
 79 local *slope* of the saturation vapor pressure curve, r_s is the assumed bulk stomatal resistance of
 80 well-watered vegetation, C_H is an assumed scalar transfer coefficient, ρ_a is the air density, c_p
 81 is the air specific heat, L_v is the heat of vaporization of water, $\gamma := (c_p p_s) / (\epsilon L_v)$, p_s is the air
 82 pressure, $\epsilon \approx 0.622$ is the ratio of molar masses of water vapor and dry air, and G is the heat flux
 83 into the ground or soil (usually ignored or parameterized).

84 In a previous study (Scheff and Frierson 2014, hereinafter SF14), the authors computed 1981-
 85 1999 and 2081-2099 annual PET climatologies for 13 GCMs in the CMIP5 (Coupled Model In-
 86 tercomparison Project phase 5) multi-model ensemble (Taylor et al. 2012), using 3-hourly sur-
 87 face output from the “historical” and business-as-usual “rcp8.5” scenarios in a procedure closely
 88 adapted from the American Society of Civil Engineers’ (ASCE) standardized tall-crop version of
 89 (1) for hourly data (Allen et al. 2005). Here we make use of those same PET climatologies, ex-
 90 panded to include the three additional CMIP5 GCMs that have since archived output satisfying the
 91 SF14 criteria. The resulting 16 models are listed in Table 1 along with any exceptions to the SF14
 92 procedures. Note that the GCM’s land-surface skin temperature T_s (as opposed to T_a) is not used
 93 in (1); instead, the derivation of (1) uses the often much cooler skin temperature of a wet surface,
 94 consistent with the definition of PET. Thus, the conceptual problem with GCM internal “PET”

95 fields identified by Milly (1992) is explicitly avoided by using the Penman-Monteith approach.
96 See Milly (1992) and section 1b of SF14.

97 In addition, we apply the SF14 procedures to 3-hourly, 1° , 1981-99 meteorological data from
98 the Global Land Data Assimilation System 2.0 (GLDAS; Rodell et al. 2004) to obtain a compara-
99 ble observational estimate of climatological PET. This data comes directly from the widely-used
100 Sheffield et al. (2006) meteorological forcing dataset, except for the upward energy fluxes used
101 to compute $(R_n - G)$ which inevitably have some influence from the Noah land model used in
102 GLDAS.

103 We also compute all of these PET climatologies using monthly-mean instead of 3-hourly out-
104 put, with a procedure closely adapted from the ASCE standardized tall-crop version of (1) for
105 daily data. This is very similar to the 3-hourly SF14 procedure; the main differences (after Allen
106 et al. 2005) are that e^* is estimated as the average of $e^*(T_{\min})$ and $e^*(T_{\max})$ where T_{\min} and T_{\max}
107 are the monthly-mean daily minimum and maximum values of T_a , that Δ is somewhat differently
108 estimated as $\Delta(T_{\text{mean}})$ where T_{mean} is the average of T_{\min} and T_{\max} , and that r_s is set to a constant
109 45 s m^{-1} . (The only other difference is that the monthly average of $|u|$ is archived directly by the
110 models as “sfcWind”, not computed from the vector components.) This is much less computation-
111 ally intensive than using 3-hourly output, and many previous studies (e.g. Feng and Fu 2013; Cook
112 et al. 2014; Dai 2013) have also used monthly-mean output, so the comparison is of considerable
113 interest. However, contrary to their stated method (Allen et al. 1998) and to Allen et al. (2005),
114 those studies simply estimated e^* as $e^*(T_{\text{mean}})$, so we also do another set of monthly PET compu-
115 tations using this non-standard e^* estimate, for comparison to our main results. (For the GLDAS
116 observations, we *only* use this non-standard method, since T_{\min} and T_{\max} are not included in the
117 GLDAS monthly product.)

118 Finally, P (unlike PET) is one of the variables directly saved by the GCMs, so we compute its
119 annual climatologies using monthly-mean output, for simplicity. We also use gauge-based obser-
120 vational estimates from the Global Precipitation Climatology Centre (GPCC) 1951-2000 climatol-
121 ogy product (Schneider et al. 2014), for comparison. (The 1981-99 mean of the less comprehensive
122 Climatic Research Unit “TS3.21” P product (Harris et al. 2014) is nearly identical.)

123 3. Results and discussion

124 *a. Basic states*

125 Fig. 1 maps the 1981-99 terrestrial P climatologies for each GCM in Table 1, with the GPCC
126 observational product also shown for reference and five key regions (defined in Table 2) outlined
127 with rectangles. One can immediately see that while in many places the models are quite similar
128 to each other and to the observations (e.g. much of Eurasia and northern Africa), in many other
129 places they differ greatly. Perhaps the most dramatic model-to-model differences are in the out-
130 lined region of northern South America (as well as neighboring Central America), where many
131 models simulate only $1\text{--}2\text{ mm day}^{-1}$ of precipitation (red and orange, similar to the Sahel or the
132 interior western United States) across the same vast areas where other models (and the observa-
133 tions) have $5\text{--}8\text{ mm day}^{-1}$ or more (blue), and dense tropical rainforests are found. The same
134 situation, where some models have near-observed large-scale P but other models have a great deal
135 less, also occurs across the central Amazon Basin and the (outlined) southeast of the continent;
136 Malhi et al. (2009) noted similar behavior in the CMIP3 models. This type of difference is also
137 particularly stark for the Indian Peninsula (also outlined), where some models have $0\text{--}1\text{ mm day}^{-1}$
138 yet most other models (and the observations) have $\sim 3\text{ mm day}^{-1}$. Conversely, through large por-
139 tions of southern Africa (outlined) and central Africa, several models simulate roughly double the

140 observed P amounts, while many other models are closer to observed. South and central China
141 and much of central North America (outlined) also have striking inter-model P disagreements.

142 Fig. 2 shows the corresponding climatologies of annual Penman-Monteith PET (computed using
143 the 3-hourly output) on the same scale. (This is simply an expansion and rescaling of SF14's Fig.
144 1, plus an observational panel.) In many of the same low-to-mid-latitude areas where the models
145 strongly disagree on P , they also strongly disagree on PET, and the high- P models are often also
146 the low-PET models in a given area. For example, in much of South America, the two MRI models
147 (and ACCESS1.0 and HadGEM2-ES to a lesser extent), which all showed high, realistic P in Fig.
148 1, also have much lower, more realistic PET, just 3-4 mm day⁻¹ (light blue) where most of the
149 other models have 5-7 mm day⁻¹ (yellow to red), much greater than observed. Similar patterns
150 of very large, opposite biases in PET and P are also common in the Southern Africa and Indian
151 Peninsula regions. This negative inter-model relationship is somewhat to be expected, since rainier
152 simulated climates also likely have less sunshine, higher relative humidity, and (in the tropics
153 and/or warm seasons) cooler daytime temperatures, all of which mean lower Penman-Monteith
154 PET (e.g. Allen et al. 2005, SF14) (see also Brutsaert and Parlange 1998). However, there are
155 also strong PET inter-model differences in Fig. 2 that do not show such a clear association with P
156 differences. For example, maximum PET values in the central Sahara, where $P \sim 0$, range from
157 6 to over 8 mm day⁻¹ (Fig. 1 of SF14 shows that some of these models exceed 10 mm day⁻¹, in
158 fact.)

159 Fig. 3 distills these relationships by taking area-weighted means of Figs. 1 and 2 over all land
160 in each region, and plotting the regional P and PET against each other. (These means are taken
161 by nearest-neighbor interpolating each model onto a common 0.25° grid and using only those
162 0.25° gridpoints which get assigned to an analyzed gridbox for *every* model, so that the same set of
163 points is used in each model despite the different coastlines.) The negative inter-model relationship

164 between mean-state P and PET is always visually clear, and the correlation is always stronger than
165 -0.6. The dramatic, zeroth-order differences between many models and the observational estimates
166 are also made clear: some models have barely half observed P for the two South American regions
167 (or nearly twice observed P for the Southern Africa region), and/or an order of magnitude less P
168 than observed for the Indian Peninsula region. The large scale of the defined regions means that
169 somewhat smaller-scale differences (e.g. across the north coast of South America) are even greater.

170 Fig. 4 shows the percent differences between the Penman-Monteith PET climatologies computed
171 using monthly-mean output (with the standard e^* estimate) and those computed using 3-hourly
172 output just shown in Fig. 2. Throughout much of the low- to mid-latitudes the monthly-computed
173 PET is higher than the 3-hourly by about 10-30%, with the exact magnitude and extent of the
174 difference varying somewhat among models. At high latitudes the difference typically takes the
175 opposite sign and is somewhat smaller. (In the two IPSL models, the discrepancy is much larger
176 and consistently positive.) The discrepancy turns out to be largely explained by a rather uniform
177 20-50% (50-150% in the IPSL models) overestimation of the aerodynamic (i.e. right-hand) term
178 of eq. (1) by the monthly method. Similar magnitude discrepancies, albeit with different signs
179 and patterns, are found for the observational estimates using the nonstandard $e^* = e^*(T_{\text{mean}})$ for
180 the monthly computations; equivalent plots for the models look similar (not shown). Thus, the
181 discrepancies are not a simple artifact of the choice of e^* estimate. We conclude that monthly-
182 computed PET, which does not account for the diurnal cycle of most variables or for weather
183 variability, is not usually representative of more carefully computed climatological PET. So, we
184 use the 3-hourly-computed PET, except where indicated.

185 Having examined the climatological terrestrial P and PET in the models and observations, Fig. 5
186 plots their ratio, the aridity index P/PET , with the UN dryland categories (Middleton and Thomas
187 1997) on the color scale. The large, reinforcing P and PET differences highlighted above generate

188 similarly stark model-dependent biases in terrestrial aridity. Vast areas of South America may
 189 be simulated as anything from semiarid/arid ($P/PET \sim 0.2$) to extremely humid ($P/PET > 1.5$)
 190 depending on the model, particularly in the humid northern and southeastern regions where ob-
 191 served P/PET is > 1.5 and ≈ 1 respectively. The central Amazon Basin, at least, is usually humid
 192 ($P/PET > 0.65$) in the models, but it is still much more so in some than others, again consistent
 193 with estimates for CMIP3 models in Malhi et al. (2009). There is also strong disagreement on
 194 aridity in central North America: some models depict a very large semi-arid area reaching up
 195 into the central/western United States and Canada, with P/PET as low as 0.3 or so, while oth-
 196 ers keep the vast majority of the United States and Canada humid, outside of the far southwest.
 197 The observations, in contrast, have a sharp west-east gradient in aridity across the highlighted
 198 region. Similarly, the Indian subcontinent in some models is a large, nearly hyper-arid desert
 199 ($P/PET \approx 0.05$) similar to the Arabian Peninsula, while in others it contains regions that range
 200 from arid to humid, in line with observations. There are also interesting large-scale differences in
 201 southern to central Africa, Australia, east China, and many other areas. These all may be of more
 202 immediate consequence to applications than the P disagreements over tropical oceans highlighted
 203 by more general reviews such as Flato et al. (2013).

204 *b. Responses to greenhouse warming*

205 Fig. 6 maps the model changes in annual terrestrial P between the 1981-99 base state described
 206 above and the 2081-99 “rcp8.5” future. As found in more general studies (e.g. Collins et al. 2013;
 207 Scheff and Frierson 2012a,b), P increases are generally widespread in high latitudes. However,
 208 the responses over mid- to low-latitude land do not neatly fit the typical description of deep-
 209 tropical increases and subtropical decreases found in those studies, which focused largely on P
 210 responses over the oceans because they tend to be more robust. Instead, these regions generally

show patterns of both increase and decrease in P that vary widely from model to model with little zonal structure. For example, in many models the region of strongest absolute terrestrial P decline is tropical northern South America, not the subtropics. In some models (e.g. the two GFDL-ESM's) P declines actually predominate throughout low- to mid-latitude land, while in others (e.g. CNRM-CM5) P increases predominate, with few declining regions. Most models are between these two extremes, but with widely varying, non-zonal patterns, particularly in South America, Africa, Australia and southern to eastern Asia, and with no particular preference for P increases or decreases outside of the high latitudes.

Interestingly, these P changes do not tend to be positively related to climatological P , P/PET or (not shown) $P - E$ across models; that is, the models that reduce P in a given location are not generally the drier ones, contrary to a “wet-get-wetter” expectation (e.g. Held and Soden 2006). For example, in northern South America HadGEM2-ES, ACCESS1-0, and the two MRI models are very humid in the mean yet have huge declines in P with greenhouse warming, and in India the two BCC and two MRI models are very arid in the mean yet show marked P increases. Fig. 7 plots regional-mean change in P against basic-state P/PET to emphasize this; substantial positive correlations are absent (central North America comes closest at +0.47, though some of the driest models there still increase P the most.) All the correlation magnitudes are much less than in Fig. 3. The x-axes of Fig. 7 span multiple UN aridity categories, again highlighting the zeroth-order model disagreements and biases in aridity discussed above.

In contrast, annual PET increases moderately but very robustly across all of the models and across all of global land, as shown in Fig. 8. This is just an expansion of Fig. 3 from SF14, but is shown here for reference. As shown by SF14, this is because the direct response of the Penman-Monteith equation to temperature at constant relative humidity dominates the responses to the other factors, and must always be positive. The physical mechanisms for this response are

the widening of the vapor pressure deficit and the increase of the equilibrium evaporative fraction, both of which come directly from the Clausius-Clapeyron equation. The percentage increases tend to be larger at higher latitudes because the percent sensitivity of (1) to temperature is much larger at cooler background temperatures, due to the lower evaporative fraction (SF14). Also, though the physical increases shown in Fig. 8 are mostly due to warming, they are much smaller than the huge, fictitious increases in PET projected by empirical temperature-based methods like the Thornthwaite equation (used in the most common version of the PDSI) and the Croley method (used in Great Lakes studies), which are clearly invalid under climate change (e.g. Hoerling et al. 2012; Lofgren et al. 2011; Hobbins et al. 2008; McKenney and Rosenberg 1993; Sheffield et al. 2012). For more details on all of this, see SF14.

Fig. 9 shows the difference between the percent changes in monthly-computed PET (using the standard e^* estimate; results with the nonstandard estimate are nearly identical) and the percent changes in 3-hourly-computed PET just shown in Fig. 8. SF14 had posited that methods not explicitly resolving the diurnal cycle (such as the use of monthly output) might strongly overestimate the PET increase, because total PET is much more sensitive to conditions during the daytime, which is when greenhouse warming is generally below its diurnal average. However, with a few high-latitude exceptions in certain models, the differences (Fig. 9) are quite small compared to the increases themselves (Fig. 8), perhaps because the diurnal dependence of greenhouse warming is not actually that large outside the high latitudes (see Fig. 10.11b of Meehl et al. 2007). This lends further confidence to the results of Feng and Fu (2013), Cook et al. (2014), Dai (2013), and other studies driven by 21st-century changes in monthly-computed Penman-Monteith PET.

Finally, Fig. 10 maps the changes in the aridity index P/PET between the two epochs. The moderate, consistent Penman-Monteith PET increases (Fig. 8) combine with the more muddled terrestrial P changes (Fig. 6) to yield widespread declines in the supply-demand ratio P/PET (i.e.

259 aridification) outside of the high latitudes, with generally fewer areas of increases in P/PET . In
260 each model, there are large areas where raw annual P (Fig. 6) increases with greenhouse warming,
261 yet when normalized by annual PET (Fig. 10) it declines instead. Fig. 10 presents a very different
262 story than the widespread “wet get wetter, dry get drier” mnemonic: terrestrial drying is dominant
263 in the wet tropics and midlatitudes, not just in the dry subtropics.

264 This is the same basic picture already described by Feng and Fu (2013), Cook et al. (2014), and
265 Dai (2013), and strongly confirms their results. However, it also has the advantages of both using
266 a very simple, transparent aridity metric (P/PET) and showing spatial results for many different
267 individual GCMs. In particular, one can see that some models tend to aridify more than others.
268 Fu and Feng (2014) suggest that such global-scale disagreements on future aridity trends stem
269 from the different phases of unforced land P variability sampled by each independent model run.
270 However, Fig. 10 makes it clear that at least some of these differences stem from fundamental
271 differences in the forced model response, since pairs of related models (e.g. MRI, IPSL, BCC,
272 GFDL-ESM) look extremely similar to each other. It seems highly unlikely in light of these close
273 similarities between independent runs that, for example, the MRI models aridify less than the
274 others because they both happen to sample an unusually wet period of natural variation during
275 2081-99. Further investigation would augment this “poor man’s ensemble” by evaluating multiple
276 runs for each model, when possible.

277 **4. Two alternative metrics**

278 One disadvantage of a plot like Fig. 10, which depicts absolute changes in P/PET as in Feng
279 and Fu (2013), is that very wet regions (e.g. the high latitudes, the Amazon, Southeast Asia) are
280 disproportionately highlighted because the magnitude of P/PET is so much larger there already.
281 Equivalently, as can be seen from the scale on Fig. 5, the same absolute P/PET change is much

282 more consequential in dry climates than in wet ones: a change from 0.6 to 0.1 implies a wholesale
 283 ecoclimatic shift from subhumid savanna or forest to arid desert, while a change from 1.6 to 1.1 is
 284 merely from rather humid forest to fairly humid forest (Budyko and Miller 1974; Holdridge 1967).
 285 This makes Fig. 10 “unfair” in some sense. Using the reciprocal PET/P , as those older studies do,
 286 merely causes the opposite, worse problem: a change from, say, 100 to 97 in a hyperarid desert
 287 is obviously much less important than a change from 3.5 to 0.5 (semiarid to very humid.) This
 288 suggests that we might look at the *relative* changes in P/PET or PET/P , in the form of percent
 289 changes (as in Fu and Feng 2014) or ratios (as suggested by the scale in Holdridge 1967). However,
 290 this still “unfairly” highlights tiny changes in very arid regions with $P \approx 0$: a chance increase from
 291 $P/PET = 0.0001$ to 0.0002 is depicted as boldly as an increase from 0.5 to 1 elsewhere, leading to
 292 rather meaningless features in places like the Sahara. (This occurs frequently in plots of percent
 293 change in P ; see Fig. 12.22 of Collins et al. (2013) for examples.)

294 Therefore, it would be useful to employ an aridity change metric whose practical meaning does
 295 not depend so strongly on the base climate. P/PET and PET/P are each fundamentally unbalanced
 296 because they approach infinity on one side but 0 on the other. One way to portray the relative mag-
 297 nitudes of climatic water supply P vs. demand PET in a more balanced (yet still nondimensional)
 298 fashion is to use the ratio $P/(P + PET)$, which just ranges between 0 ($PET \gg P$) and 1 ($P \gg PET$).
 299 Like the division of P and PET in the traditional index, the addition of P and PET in the denom-
 300 inator is not physical in and of itself but just helps us numerically assess the relative magnitudes.
 301 A similar approach is sometimes taken in terrestrial plant modeling (e.g. Medvigy et al. 2009).

302 Our new index $P/(P + PET)$ is a one-to-one function of P/PET or PET/P ,

$$\frac{P}{P + PET} = \frac{P/PET}{P/PET + 1} = \frac{1}{1 + PET/P}, \quad (2)$$

so it preserves exactly the same information: $P/PET = 1$ always corresponds to $P/(P + PET) = 1/2$, $P/PET = 0.2$ to $P/(P + PET) = 1/6$, and so on. However, as desired, change magnitudes are not one-to-one: the above P/PET change from 0.6 to 0.1 corresponds to a $P/(P + PET)$ change from 0.38 to 0.09, while the “equal” P/PET change from 1.6 to 1.1 corresponds to a $P/(P + PET)$ change from just 0.62 to 0.52, nearly three times smaller than the first change. Essentially, $P/PET = 0.6$ to 0.1 represents a more dramatic change in our assessment of whether $PET \gg P$, $P \gg PET$, or $P \sim PET$ than does $P/PET = 1.6$ to 1.1.

Inspired by this reasoning, Fig. 11 plots this alternate aridity index $P/(P + PET)$ for each model, using the 1981-99 climatologies. As expected, it is in a one-to-one relationship with Fig. 5 (as shown on the scale), with the same spatial patterns and model-to-model differences apparent. However, the boundaries between UN dryland categories now occur at somewhat more regular intervals, and the scale is now able to saturate at more humid climates ($P/PET = 5$ rather than 1.5) due to the compression, allowing more information to be retained without sacrificing any detail in the drier climates. The scale also provides a handy reference for converting between the two indices.

Fig. 12 then maps the changes in $P/(P + PET)$ between the 2081-99 and 1981-99 periods. As desired, the magnitudes are more spatially comparable than in Fig. 10, with high-latitude changes in particular becoming much less saturated, and subtropical changes becoming less washed-out. Of course, the signs of the changes are still the same. If anything, the reduction in distracting wet-zone “noise” makes the overall global trend toward aridity in most models, and the fact that some models somewhat buck that trend, even clearer. The uniformly applicable scale also makes the changes more striking: everywhere that the color saturates, the modeled P vs. PET balance is moving $\sim 1/6$ or more of the way from $P \gg PET$ to $PET \gg P$ or vice versa, the same as a change from semiarid to arid, or alternatively from Seattle ($P/(P + PET) = 0.53$) to Dal-

327 las ($P/(P + PET) = 0.38$.) Aridification of this magnitude seems to occur particularly often in
 328 the Amazon, southern Europe, and in Mexico and vicinity, but can happen in many diverse ter-
 329 restrial locations depending on the model. Similarly, humidification of this magnitude is most
 330 commonly projected in parts of Siberia, but can also occur in parts of South America, Africa or in
 331 subarctic North America, depending on the model. However, even the more ordinarily projected
 332 $P/(P + PET)$ change magnitudes of 0.05 to 0.10 are clearly consequential on the scale of Fig.
 333 11, and the wide prevalence of $P/(P + PET)$ declines of this magnitude throughout the tropics,
 334 subtropics and midlatitudes is a worrisome prediction.

335 Another common 0-to-1-valued terrestrial wetness metric is the *evaporative fraction*
 336 $LH/(LH + SH)$ (e.g. Koster et al. 2009; Gentine et al. 2011), the proportion of total upward tur-
 337 bulent heat flux made up by evaporation or latent heat (LH) rather than sensible heat (SH). As
 338 with $P/(P + PET)$, values closer to 1 imply more well-watered conditions, while values closer to
 339 0 are consistent with insufficient water. $LH/(LH + SH)$ is also an exact nonlinear function of the
 340 better-known but worse-behaved Bowen ratio SH/LH , just as $P/(P + PET)$ is to PET/P . How-
 341 ever, unlike $P/(P + PET)$, the evaporative fraction is not purely a *climate* metric: LH and SH are
 342 at least proximately determined by the vegetation and soil, though their sum is constrained by the
 343 surface radiation balance. Equivalently, GCM (and GLDAS) LH and SH fields are produced by
 344 the *land* model, not by the atmospheric model (or data), and GCM land models still have great
 345 difficulty reproducing realistic LH (e.g. Sheffield and Coauthors 2013).

346 However, it is still instructive to compare the two metrics. Fig. 13 plots $LH/(LH + SH)$ for each
 347 GCM and for the GLDAS, where LH and SH are 1981-99 annual means. The broad spatial patterns
 348 are quite similar to Fig. 11, with higher values in the tropics and high latitudes and lower values
 349 in the subtropical dry zones, although there is an unexplained tendency for lower $LH/(LH + SH)$
 350 values in GLDAS than in the GCMs, especially at higher latitudes. By plotting regional means

of the two metrics against each other, Fig. 14 shows that $P/(P + PET)$ and $LH/(LH + SH)$ also agree extremely well on which GCMs are drier vs. wetter in a given location; the correlations are always at least +0.89. This reassuringly implies that the GCM land models are consistently responding to climate forcing, though the unusually low $LH/(LH + SH)$ values in GLDAS for a given $P/(P + PET)$ are still apparent.

Will greenhouse warming responses of $LH/(LH + SH)$ also follow greenhouse warming responses of $P/(P + PET)$? One might not expect so, since for a constant surface-wetness state, $LH/(LH + SH)$ fundamentally increases with warming due to the Clausius-Clapeyron equation (e.g. Hartmann 1994). For example, $LH/(LH + SH)$ is much higher over tropical oceans than over high-latitude oceans, even though they are equally “wet.” This could offset some of the expected drying-induced declines in $LH/(LH + SH)$. Indeed, Fig. 15 shows that unlike $P/(P + PET)$ in Fig. 12, $LH/(LH + SH)$ variously increases or decreases with projected warming in the GCMs, with no clear sign preference. However, this neutrality still implies drying with warming, since warming *alone* (without any surface drying) would lead to systematic *increases* in $LH/(LH + SH)$ as explained above. Also, the geographic patterns of the responses in Figs. 12 and 15 appear quite similar, though the signs may be different. Fig. 16 shows that regional intermodel disagreements are also very consistent between $P/(P + PET)$ responses and $LH/(LH + SH)$ responses, just as they were for the metrics’ mean states; intermodel correlations are at least +0.86 in each region. Thus, in GCMs, the atmosphere/hydroclimate response to greenhouse warming seems very relevant for the land hydrologic response, increasing our confidence in the land models.

5. Summary and conclusions

The aridity of a terrestrial climate is generally quantified using the relative magnitudes of precipitation P and potential evapotranspiration PET. This study evaluates the climatologies and

greenhouse-warming responses of terrestrial P , Penman-Monteith PET (1), and their dimensionless ratio P/PET (the *aridity index*) in 16 different CMIP5 global climate models. The climatologies generally agree in much of Eurasia and North Africa, but they disagree dramatically in large areas of the Americas, sub-Saharan Africa, South Asia, and elsewhere, with the same areas represented as semiarid-to-arid or quite humid by different models (Figs. 1, 2, 3, 5 and 7). In many of these areas, P and PET are much closer to the observations in some models than in others, and PET is often high in the same models for which P is low, strengthening the P/PET disagreements and biases.

The terrestrial P responses to warming tend to be positive at high latitudes, but an inconsistent and complex mixture of positive and negative elsewhere, counter to both naive expectations of more P in a warmer climate and ocean-inspired theories of strongly zonal P response to warming (Fig. 6). Since the Penman-Monteith PET responses to warming are uniformly and substantially positive in contrast (SF14 and Fig. 8), aridification (P/PET decline) generally dominates over humidification (P/PET increase) in the tropics, the subtropics and the midlatitudes (Fig. 10), with varying spatial patterns. This is in marked contrast to the expectation from a “wet get wetter, dry get drier” rule, but strongly agrees with more recent studies (Dai 2013; Feng and Fu 2013; Cook et al. 2014). However, this global drying tendency is much less apparent in certain models.

The PET climatologies are also found to be sensitive to the computation timescale: except at high latitudes, the aerodynamic (right-hand) part of (1) is uniformly 20-50% higher when computed using monthly rather than 3-hourly GCM output, making total PET 10-30% higher in large areas (Fig. 4). However, contrary to the authors’ earlier suggestion (SF14), the responses to greenhouse warming are not as sensitive to this choice of input timescale, though there are large local differences in some models (Fig. 9). The use of diurnally averaged temperature to estimate the monthly-mean saturation vapor pressure e^* (as done by the above studies, counter to standard pro-

cedure) does not change the general magnitude of any of these comparisons, though the details for the climatologies differ.

The same change in P/PET is much more meaningful when P/PET is low than when it is high. Therefore, an alternative index $P/(P + PET)$ (Fig. 11), which carries the same information as P/PET but only varies from 0 ($PET \gg P$) to 1 ($P \gg PET$), is also used to quantify the model aridities and responses to warming. Indeed, the responses of $P/(P + PET)$ (Fig. 12) are more spatially comparable than those of P/PET (Fig. 10), with a more uniform interpretation. This alternative method better highlights aridity changes in all terrestrial regions, rather than disproportionately focusing on changes in wet or very dry places. These $P/(P + PET)$ climatologies and changes are also consistent in many ways with evaporative fraction ($LH/(LH + SH)$) climatologies and changes (Figs. 13-16), though the latter are fundamentally biased positive by the warming itself apart from any water-availability change, obscuring the aridity-related signal (Fig. 15).

One problem with this study, and with all the cited studies that use PET to think about the terrestrial response to greenhouse warming, is that PET is just a notional flux: it is never actually realized, except in irrigated or very humid settings. The authors are in the process of developing a new framework for thinking about the effect of warming when actual $ET < PET$. Preliminary results suggest that if the actual evaporative fraction is much less than the notional evaporative fraction from a wet surface, then the actual ET requirement for plants will have a *higher* percentage sensitivity to warming than will PET, because it will be less energetically constrained. Thus, the warming-drying result may become even stronger in this framework. However, it is also important to note that ambient carbon dioxide increases might reduce plant ET requirements (e.g. Sellers et al. 1996), introducing the opposite effect. Much more work needs to be done.

Finally, it is often suggested in the paleoclimate literature that warm greenhouse climates of the past are well-watered and cold climates such as the last glacial maximum are arid, contrary to the

conclusions above. Could model biases, either in land parameterizations or atmospheric physics parameterizations, be exaggerating the global drying tendency? The authors have work planned and in progress attempting to reconcile these perspectives with a combination of paleoclimate model analysis, moisture proxy meta-analysis, and idealized climate modeling. The resolution of this dilemma could greatly improve our understanding of the future of terrestrial aridity.

Acknowledgments. We acknowledge the World Climate Research Programme’s Working Group on Coupled Modelling, which is responsible for CMIP, and we thank the climate modeling groups (listed in Table 1 of this paper) for producing and making available their model output. For CMIP the U.S. Department of Energy’s Program for Climate Model Diagnosis and Intercomparison provides coordinating support and led development of software infrastructure in partnership with the Global Organization for Earth System Science Portals. J. S. would also like to thank the two anonymous reviewers for suggestions that greatly strengthened this paper. This work was supported by NSF awards AGS-0846641, AGS-0936059, AGS-1359464, AGS-1433551, and PLR-1341497.

References

- Allen, R. G., L. S. Pereira, D. Raes, and M. Smith, 1998: Crop evapotranspiration: guidelines for computing crop water requirements. Irrigation and Drainage Paper 56, Food and Agriculture Organization.
- Allen, R. G., I. A. Walter, R. Elliott, T. Howell, D. Itenfisu, and M. Jensen, 2005: *The ASCE Standardized Reference Evapotranspiration Equation*. American Society of Civil Engineers, 59 pp.
- Brutsaert, W., and M. B. Parlange, 1998: Hydrologic cycle explains the evaporation paradox. *Nature*, **396**, 30.

- 444 Budyko, M. I., and D. H. Miller, 1974: *Climate and Life*. Academic Press, 508 pp.
- 445 Collins, M., and Coauthors, 2013: Long-term climate change: projections, commitments and
446 irreversibility. *Climate Change 2013: The Physical Science Basis. Contribution of Working
447 Group I to the Fifth Assessment Report of the Intergovernmental Panel on Climate Change*,
448 T. Stocker, D. Qin, G.-K. Plattner, M. Tignor, S. Allen, J. Boschung, A. Nauels, Y. Xia, V. Bex,
449 and P. Midgley, Eds., Cambridge University Press, 1029–1136.
- 450 Cook, B. I., J. E. Smerdon, R. Seager, and S. Coats, 2014: Global warming and 21st century
451 drying. *Climate Dyn.*, **43**, 2607–2627, doi:10.1007/s00382-014-2075-y.
- 452 Dai, A., 2013: Increasing drought under global warming in observations and models. *Nature Clim.
453 Change*, **3**, 52–58, doi:10.1038/NCLIMATE1633.
- 454 Feng, S., and Q. Fu, 2013: Expansion of global drylands under a warming climate. *Atmos. Chem.
455 Phys.*, **13**, 10 08110 094, doi:10.5194/acp-13-10081-2013.
- 456 Flato, G., and Coauthors, 2013: Evaluation of climate models. *Climate Change 2013: The Physi-
457 cal Science Basis. Contribution of Working Group I to the Fifth Assessment Report of the Inter-
458 governmental Panel on Climate Change*, T. Stocker, D. Qin, G.-K. Plattner, M. Tignor, S. Allen,
459 J. Boschung, A. Nauels, Y. Xia, V. Bex, and P. Midgley, Eds., Cambridge University Press, 741–
460 866.
- 461 Food and Agriculture Organization, 2004: Global map of monthly reference evapotranspiration
462 - 10 arc minutes. [Available online at <http://www.fao.org/geonetwork/srv/en/main.home>, June
463 2014.].
- 464 Fu, Q., and S. Feng, 2014: Responses of terrestrial aridity to global warming. *J. Geophys. Res.*,
465 **119**, 7863–7875, doi:10.1002/2014JD021608.

466 Gentine, P., D. Entekhabi, and J. Polcher, 2011: The diurnal behavior of evaporative fraction in
467 the soil-vegetation-atmospheric boundary layer continuum. *J. Hydrometeor.*, **12**, 1530–1546.

468 Harris, I., P. D. Jones, T. J. Osborn, and D. H. Lister, 2014: Updated high-resolution grids of
469 monthly climatic observations - the CRU TS3.10 dataset. *Int. J. Climatol.*, **34**, 623–642, doi:
470 10.1002/joc.3711.

471 Hartmann, D., 1994: *Global Physical Climatology*. Academic Press, 411 pp.

472 Held, I., and B. Soden, 2006: Robust responses of the hydrological cycle to global warming. *J.*
473 *Climate*, **19**, 5686–5699.

474 Hobbins, M. T., A. Dai, M. L. Roderick, and G. D. Farquhar, 2008: Revisiting the parameterization
475 of potential evaporation as a driver of long-term water balance trends. *Geophys. Res. Lett.*, **35**,
476 L12403, doi:10.1029/2008GL033840.

477 Hoerling, M. P., J. K. Eischeid, X.-W. Quan, H. F. Diaz, R. S. Webb, R. M. Dole, and D. R.
478 Easterling, 2012: Is a transition to semipermanent drought conditions imminent in the U.S.
479 Great Plains? *J. Climate*, **25**, 8380–8386, doi:10.1175/JCLI-D-12-00449.1.

480 Holdridge, L. R., 1967: *Life Zone Ecology*. Tropical Science Center, 206 pp.

481 Koster, R. D., S. D. Schubert, and M. J. Suarez, 2009: Analyzing the concurrence of meteorolog-
482 ical droughts and warm periods, with implications for the determination of evaporative regime.
483 *J. Climate*, **22**, 3331–3341, doi:10.1175/2008JCLI2718.1.

484 Lofgren, B. M., T. S. Hunter, and J. Wilbarger, 2011: Effects of using air temperature as a proxy
485 for potential evapotranspiration in climate change scenarios of Great Lakes basin hydrology. *J.*
486 *Great Lakes Res.*, **37**, 744–752, doi:10.1016/j.jglr.2011.09.006.

- 487 Malhi, Y., and Coauthors, 2009: Exploring the likelihood and mechanism of a climate-change-
488 induced dieback of the Amazon rainforest. *Proc. Natl. Acad. Sci. (USA)*, **106**, 20 610–20 615,
489 doi:10.1073/pnas.084619106.
- 490 McKenney, M. S., and N. J. Rosenberg, 1993: Sensitivity of some potential evapotranspiration
491 estimation methods to climate change. *Agric. For. Meteorol.*, **64**, 81–110.
- 492 Medvigy, D., S. C. Wofsy, J. W. Munger, D. Y. Hollinger, and P. R. Moorcroft, 2009: Mechanistic
493 scaling of ecosystem function and dynamics in space and time: Ecosystem Demography model
494 version 2. *J. Geophys. Res.*, **114**, G01 002, doi:10.1029/2008JG000812.
- 495 Meehl, G. A., and Coauthors, 2007: Global climate projections. *Climate Change 2007: The Phys-
496 ical Science Basis. Contribution of Working Group I to the Fourth Assessment Report of the In-
497 tergovernmental Panel on Climate Change*, S. Solomon, D. Qin, M. Manning, Z. Chen, M. Mar-
498 quis, K. B. Averyt, M. Tignor, and H. L. Miller, Eds., Cambridge University Press, 747–845.
- 499 Middleton, N., and D. S. G. Thomas, 1997: *World Atlas of Desertification*. 2nd ed., Wiley, 182 pp.
- 500 Milly, P. C. D., 1992: Potential evaporation and soil moisture in general circulation models. *J.
501 Climate*, **5**, 209–226.
- 502 Monteith, J. L., 1981: Evaporation and surface temperature. *Q. J. R. Meteorol. Soc.*, **107**, 1–27.
- 503 Mortimore, M., 2009: *Dryland Opportunities: A new paradigm for people, ecosys-
504 tems and development*. IUCN, IIED, and UNDP/DDC, 86 pp., [Available online at
505 pubs.iied.org/pdfs/G02572.pdf].
- 506 Rodell, M., and Coauthors, 2004: The Global Land Data Assimilation System. *Bull. Amer. Meteor.
507 Soc.*, **85**, 381–394.

508 Scheff, J., and D. Frierson, 2012a: Twenty-first-century multimodel subtropical precipitation de-
 509 clines are mostly midlatitude shifts. *J. Climate*, **25**, 4330–4347, doi:10.1175/JCLI-D-11-00393.
 510 1.

511 Scheff, J., and D. M. W. Frierson, 2012b: Robust future precipitation declines in CMIP5 largely
 512 reflect the poleward expansion of model subtropical dry zones. *Geophys. Res. Lett.*, **39**, L18 704,
 513 doi:10.1029/2012GL052910.

514 Scheff, J., and D. M. W. Frierson, 2014: Scaling potential evapotranspiration with greenhouse
 515 warming. *J. Climate*, **27**, 1539–1558, doi:10.1175/JCLI-D-13-00233.1.

516 Schneider, U., A. Becker, P. Finger, A. Meyer-Christoffer, M. Ziese, and B. Rudolf, 2014:
 517 GPCC’s new land surface precipitation climatology based on quality-controlled in situ data
 518 and its role in quantifying the global water cycle. *Theor. Appl. Climatology*, **115**, 15–40, doi:
 519 10.1007/s00704-013-0860-x.

520 Sellers, P., and Coauthors, 1996: Comparison of radiative and physiological effects of doubled
 521 atmospheric CO₂ on climate. *Science*, **271**, 1402–1406.

522 Sheffield, J., and Coauthors, 2013: North American climate in CMIP5 experiments. Part I: eval-
 523 uation of historical simulations of continental and regional climatology. *J. Climate*, **26**, 9209–
 524 9245, doi:10.1175/JCLI-D-12-00592.1.

525 Sheffield, J., G. Goteti, and E. F. Wood, 2006: Development of a 50-yr high-resolution global
 526 dataset of meteorological forcings for land surface modeling. *J. Climate*, **19**, 3088–3111.

527 Sheffield, J., E. F. Wood, and M. L. Roderick, 2012: Little change in global drought over the past
 528 60 years. *Nature*, **491**, 435–438, doi:10.1038/nature11575.

529 Taylor, K. E., R. J. Stouffer, and G. A. Meehl, 2012: An overview of CMIP5 and the experiment
530 design. *Bull. Amer. Meteorol. Soc.*, **93**, 485–498, doi:10.1175/BAMS-D-11-00094.1.

531 Transeau, E. N., 1905: Forest centers of eastern America. *Amer. Naturalist*, **39**, 875–889.

532	LIST OF TABLES	
533	Table 1. CMIP5 models analyzed in this study	28
534	Table 2. Region definitions	29

TABLE 1. CMIP5 models analyzed in this study

Model acronym	Expansion and origin
ACCESS1.0 ¹	Australian Community Climate and Earth System Simulator version 1.0
BCC-CSM1.1	Beijing Climate Center (BCC), Climate System Model version 1.1, low resolution
BCC-CSM1.1-M	BCC, Climate System Model version 1.1, medium resolution
BNU-ESM	Beijing Normal University, Earth System Model
CNRM-CM5	Centre National de Recherches Météorologiques (France), Coupled Global Climate Model version 5
GFDL-CM3	NOAA Geophysical Fluid Dynamics Laboratory (GFDL), Climate Model version 3
GFDL-ESM2G	GFDL, Earth System Model version 2, using Generalized Ocean Layer Dynamics
GFDL-ESM2M	GFDL, Earth System Model version 2, using Modular Ocean Model
GISS-E2-H ²³	NASA Goddard Institute for Space Studies (GISS), ModelE version 2, using Hybrid Coordinate Ocean Model
GISS-E2-R ²³	GISS, ModelE version 2, using Russell ocean model
HadGEM2-ES ¹⁴⁵	Met Office Hadley Centre (UK), Global Environment Model version 2, Earth System configuration
INM-CM4	Institute for Numerical Mathematics (Russia), Coupled Model version 4
IPSL-CM5A-LR	L’Institut Pierre-Simon Laplace (IPSL) (France), Coupled Model version 5, NEMO ocean, low resolution
IPSL-CM5A-MR	IPSL, Coupled Model version 5, NEMO ocean, medium resolution
MRI-CGCM3	Meteorological Research Institute (MRI) (Japan), Coupled Atmosphere-Ocean General Circulation Model version 3
MRI-ESM1	MRI, Earth System Model version 1

¹Surface winds were given on a grid staggered from that of the other surface variables; see the appendix of SF14.

²Version with interactive aerosols and chemistry (“p3”) is shown here; results for version with prescribed aerosols and chemistry (“p1”) were nearly identical.

³Run 6 was used for historical and run 2 was used for rcp8.5, as these were the only respective runs with 3-hourly output.

⁴Run 2 was used for historical (and run 1 was used for rcp8.5), as these were the only respective runs with 3-hourly output.

⁵3-hourly surface pressure was not available, so monthly surface pressure output was used for each 3-hour interval.

TABLE 2. Region definitions

Northern South America	45°-70°W, 10°S-10°N
Southeast South America	45°-60°W, 35°-15°S
Central North America	90°-110°W, 30°-50°N
Indian Peninsula	70°-85°E, 10°-25°N
Southern Africa	15°-35°E, 35°-10°S

535	LIST OF FIGURES	
536	Fig. 1.	1981-99 climatological annual-mean precipitation P in mm day^{-1} for each CMIP5 model in
537		Table 1, with Global Precipitation Climatology Centre gauge-based observational product
538		as described in section 2. Values in a few color-saturated regions greatly exceed those on
539		the scale. Regions in Table 2 are outlined. 32
540	Fig. 2.	1981-99 annual-mean potential evapotranspiration (PET) in mm day^{-1} for each model and
541		for the Global Land Data Assimilation System 2.0 (GLDAS) observation-based product as
542		described in section 2. 33
543	Fig. 3.	1981-99 annual-mean regional-land-mean P vs. PET for each model (numbers) and for the
544		observational products (asterisk), plotted for each region in Table 2. Values in parentheses
545		are simple correlations of the 16 model points. 34
546	Fig. 4.	Percent differences between the 1981-99 annual-mean PET computed using monthly vs.
547		3-hourly output, for each model and for the GLDAS observation-based product. For the
548		observations only, the nonstandard $e^* = e^*(T_{\text{mean}})$ is used in the monthly computation. . . . 35
549	Fig. 5.	1981-99 aridity index P/PET for each model and for the observational products, where
550		P and PET are the climatologies shown in Figs. 1 and 2. The dryland categories from
551		Middleton and Thomas (1997) are indicated on the scale (HA = hyperarid; DSH = dry
552		subhumid; above 0.65 is considered humid.) 36
553	Fig. 6.	Changes in annual precipitation P in mm day^{-1} between 1981-99 (“historical” scenario) and
554		2081-99 (“rcp8.5” scenario), for each model. 37
555	Fig. 7.	Regional-land-mean 1981-99 aridity index P/PET vs. 21st-century P change, for each
556		model and region. Values in parentheses are simple correlations of the model points. The
557		dashed line is observational regional-land-mean P/PET . For reference, P/PET less than
558		0.05 is defined as hyperarid, 0.05 to 0.2 as arid, 0.2 to 0.5 as semiarid, 0.5 to 0.65 as dry
559		subhumid, and more than 0.65 as humid (Middleton and Thomas 1997); see the scale of Fig.
560		5. 38
561	Fig. 8.	Percent changes in annual PET between 1981-99 and 2081-99, for each model. 39
562	Fig. 9.	Differences between the percent changes in annual PET over the 21st century computed
563		using monthly vs. 3-hourly output. 40
564	Fig. 10.	Changes in the aridity index P/PET between 1981-99 and 2081-99, for each model. 41
565	Fig. 11.	1981-99 alternate aridity index $P/(P + \text{PET})$ (right-hand scale) for each model and for the
566		observations. The corresponding P/PET values (left-hand scale) and dryland categories are
567		also shown for reference. Compare to Fig. 5. 42
568	Fig. 12.	Changes in the alternate aridity index $P/(P + \text{PET})$ between 1981-99 and 2081-99, for each
569		model. 43
570	Fig. 13.	1981-99 evaporative fraction $\text{LH}/(\text{LH} + \text{SH})$ for each model and for the GLDAS
571		observation-driven land model estimate. 44
572	Fig. 14.	1981-99 regional-land-mean alternate aridity index $P/(P + \text{PET})$ vs. evaporative fraction
573		$\text{LH}/(\text{LH} + \text{SH})$ for each model (numbers) and for the observational products (asterisk), for

574	each region. Values in parentheses are simple correlations of the 16 model points. For	
575	reference, $P/(P + PET)$ less than ≈ 0.05 is defined as hyperarid, ≈ 0.05 to $1/6$ as arid, $1/6$	
576	to $1/3$ as semiarid, $1/3$ to ≈ 0.39 as dry subhumid, and more than ≈ 0.39 as humid; see the	
577	scale of Fig. 11.	45
578	Fig. 15. Changes in evaporative fraction $LH/(LH + SH)$ between 1981-99 and 2081-99, for each	
579	model.	46
580	Fig. 16. Regional-land-mean 21st-century $P/(P + PET)$ change vs. $LH/(LH + SH)$ change, for each	
581	model and region. Values in parentheses are simple correlations of the model points.	47

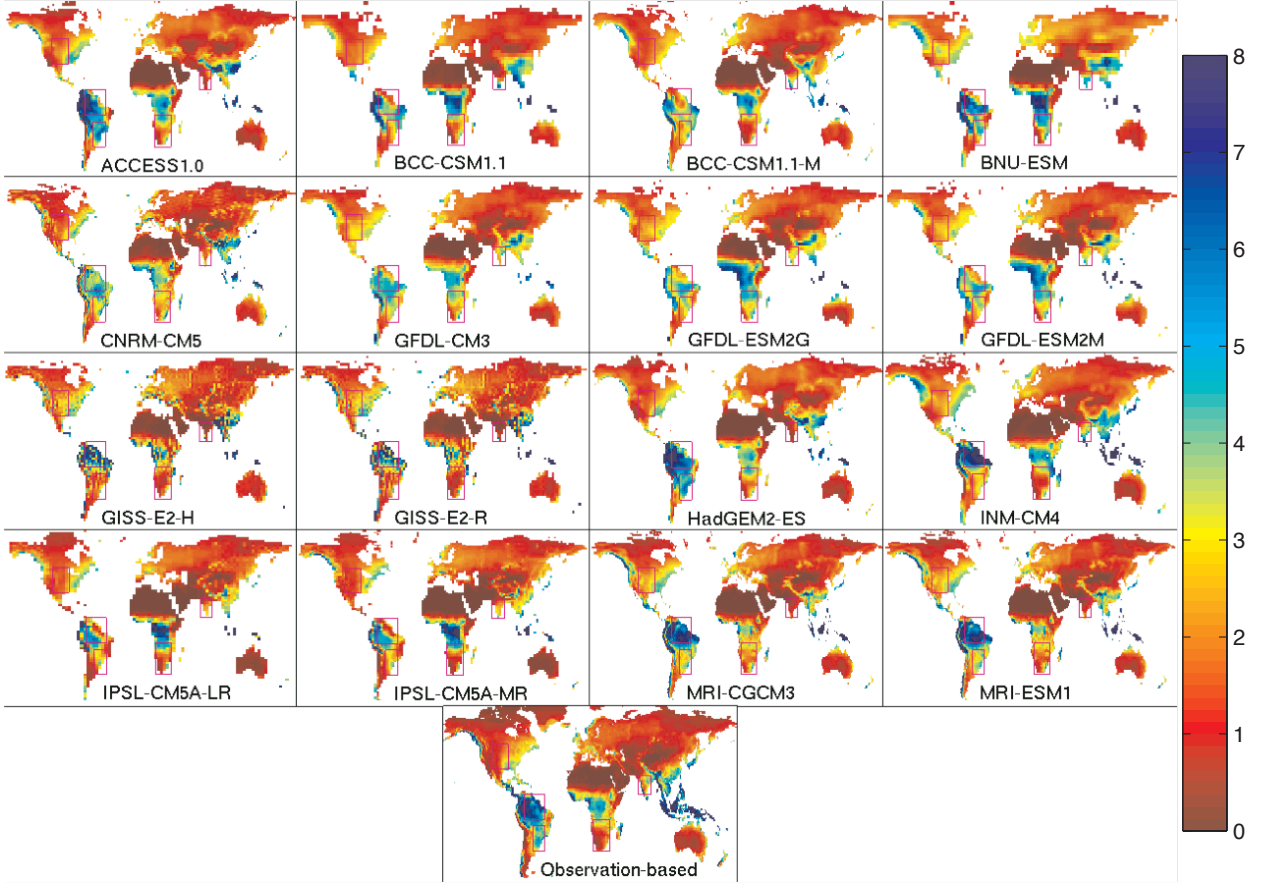


FIG. 1. 1981-99 climatological annual-mean precipitation P in mm day^{-1} for each CMIP5 model in Table 1, with Global Precipitation Climatology Centre gauge-based observational product as described in section 2. Values in a few color-saturated regions greatly exceed those on the scale. Regions in Table 2 are outlined.

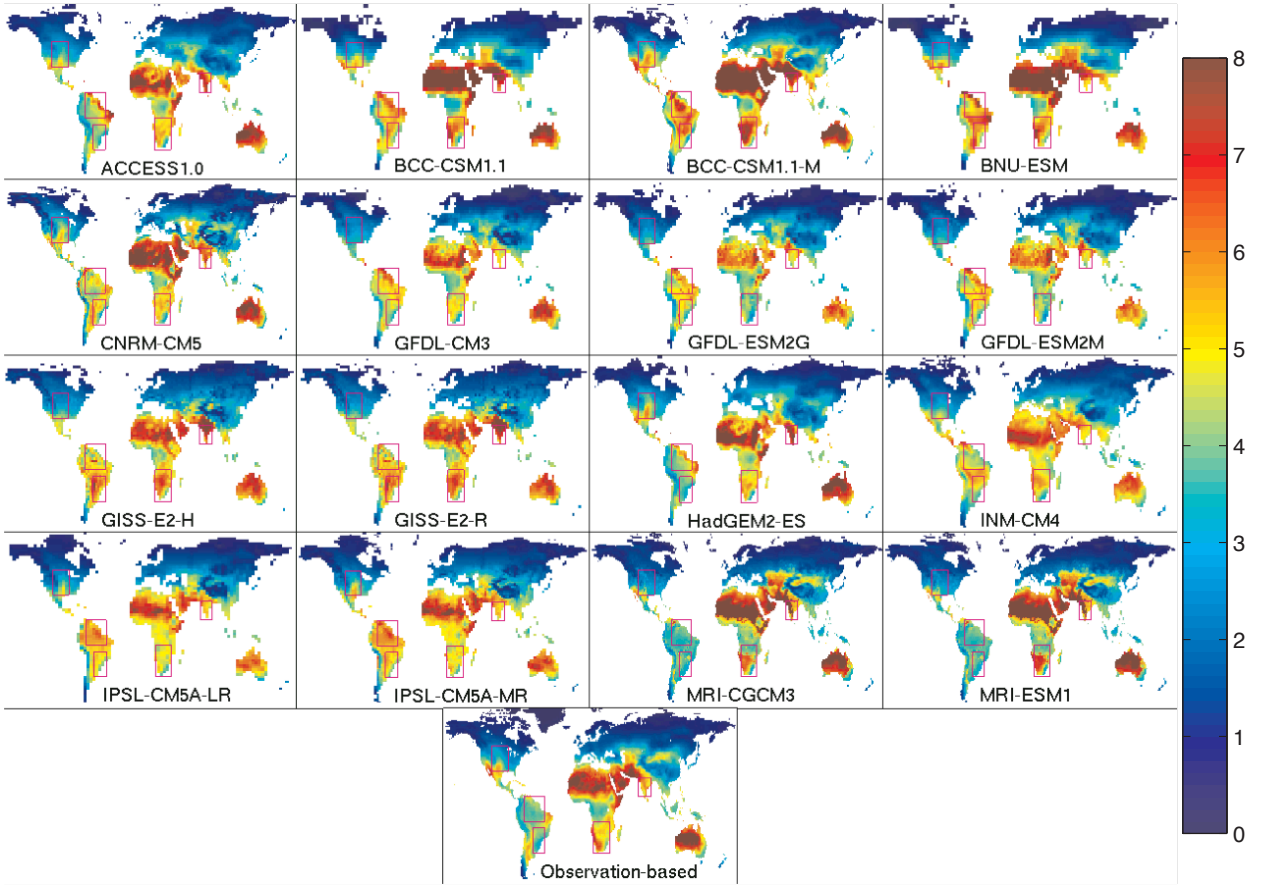


FIG. 2. 1981-99 annual-mean potential evapotranspiration (PET) in mm day^{-1} for each model and for the
Global Land Data Assimilation System 2.0 (GLDAS) observation-based product as described in section 2.

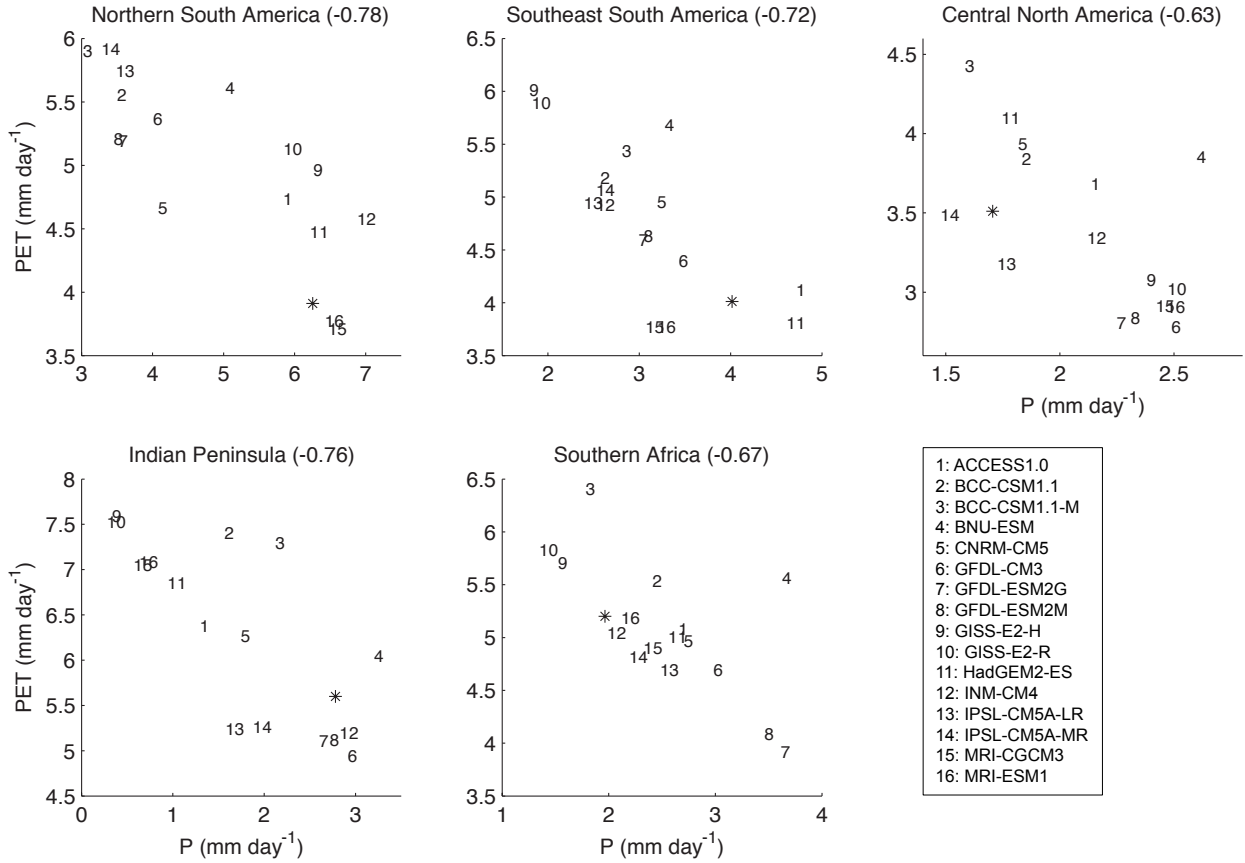


FIG. 3. 1981-99 annual-mean regional-land-mean P vs. PET for each model (numbers) and for the observational products (asterisk), plotted for each region in Table 2. Values in parentheses are simple correlations of the 16 model points.

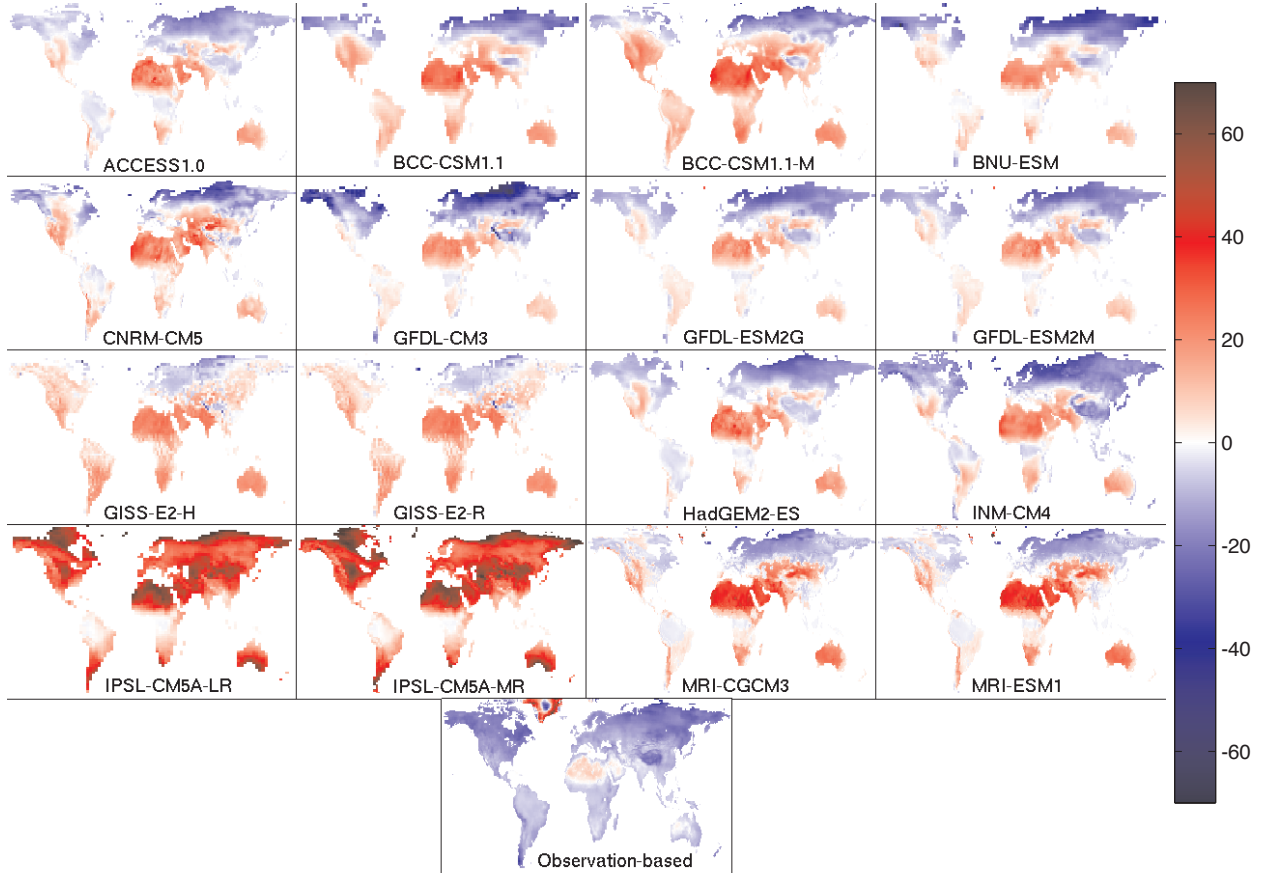


FIG. 4. Percent differences between the 1981-99 annual-mean PET computed using monthly vs. 3-hourly output, for each model and for the GLDAS observation-based product. For the observations only, the nonstandard $e^* = e^*(T_{\text{mean}})$ is used in the monthly computation.

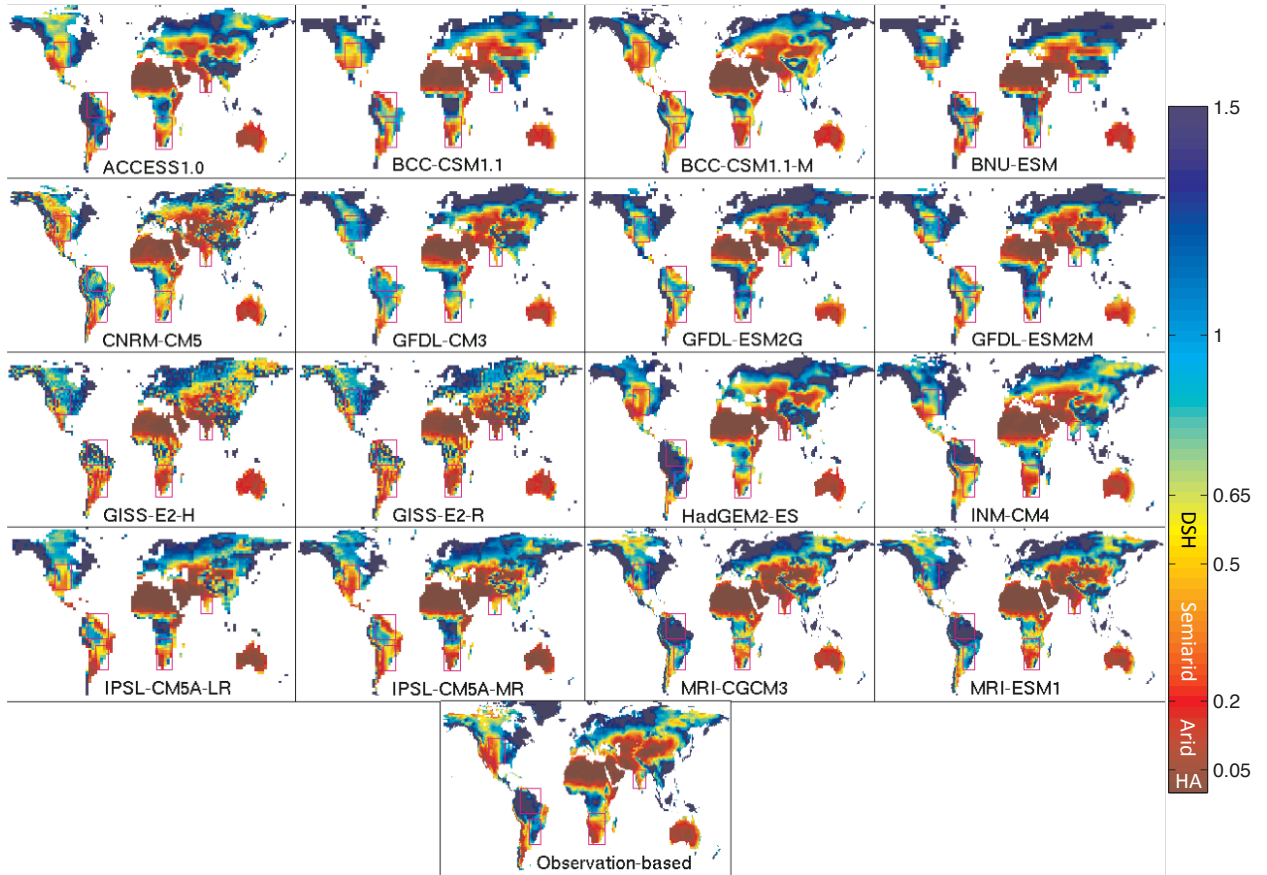
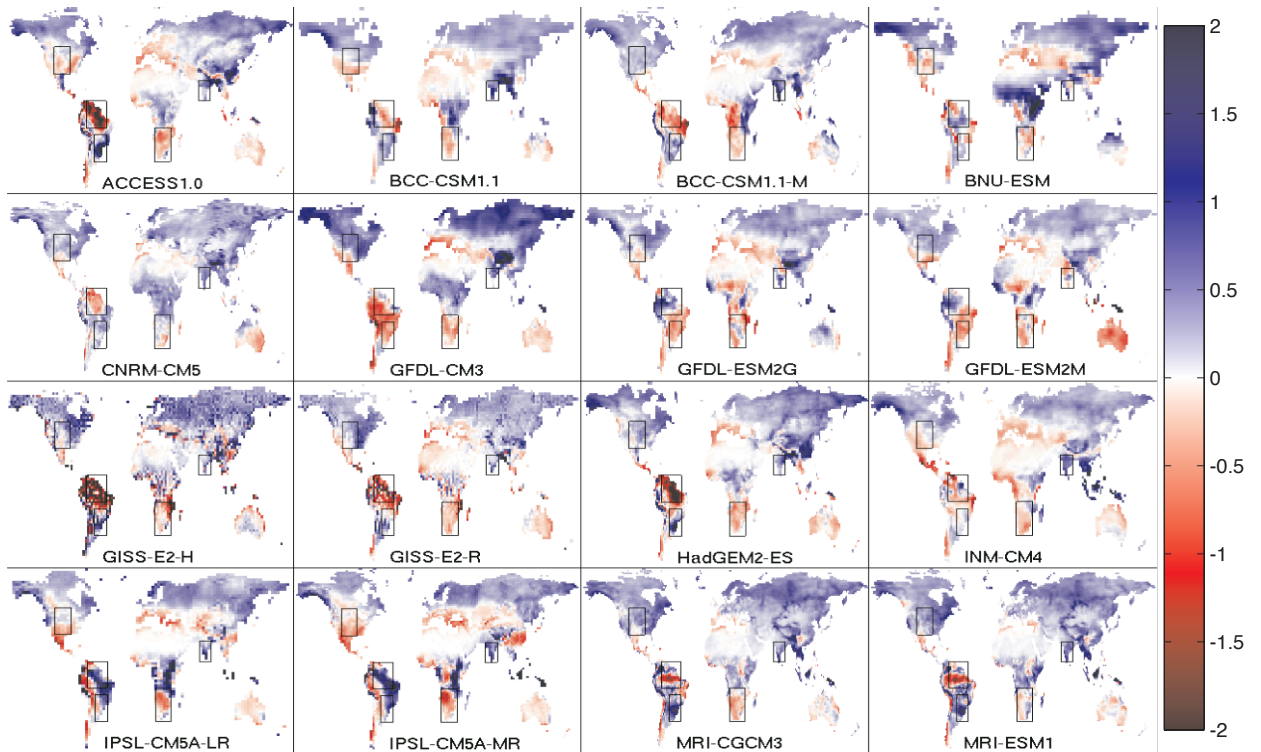


FIG. 5. 1981-99 aridity index P/PET for each model and for the observational products, where P and PET are the climatologies shown in Figs. 1 and 2. The dryland categories from Middleton and Thomas (1997) are indicated on the scale (HA = hyperarid; DSH = dry subhumid; above 0.65 is considered humid.)



596 FIG. 6. Changes in annual precipitation P in mm day^{-1} between 1981-99 (“historical” scenario) and 2081-99
 597 (“rcp8.5” scenario), for each model.

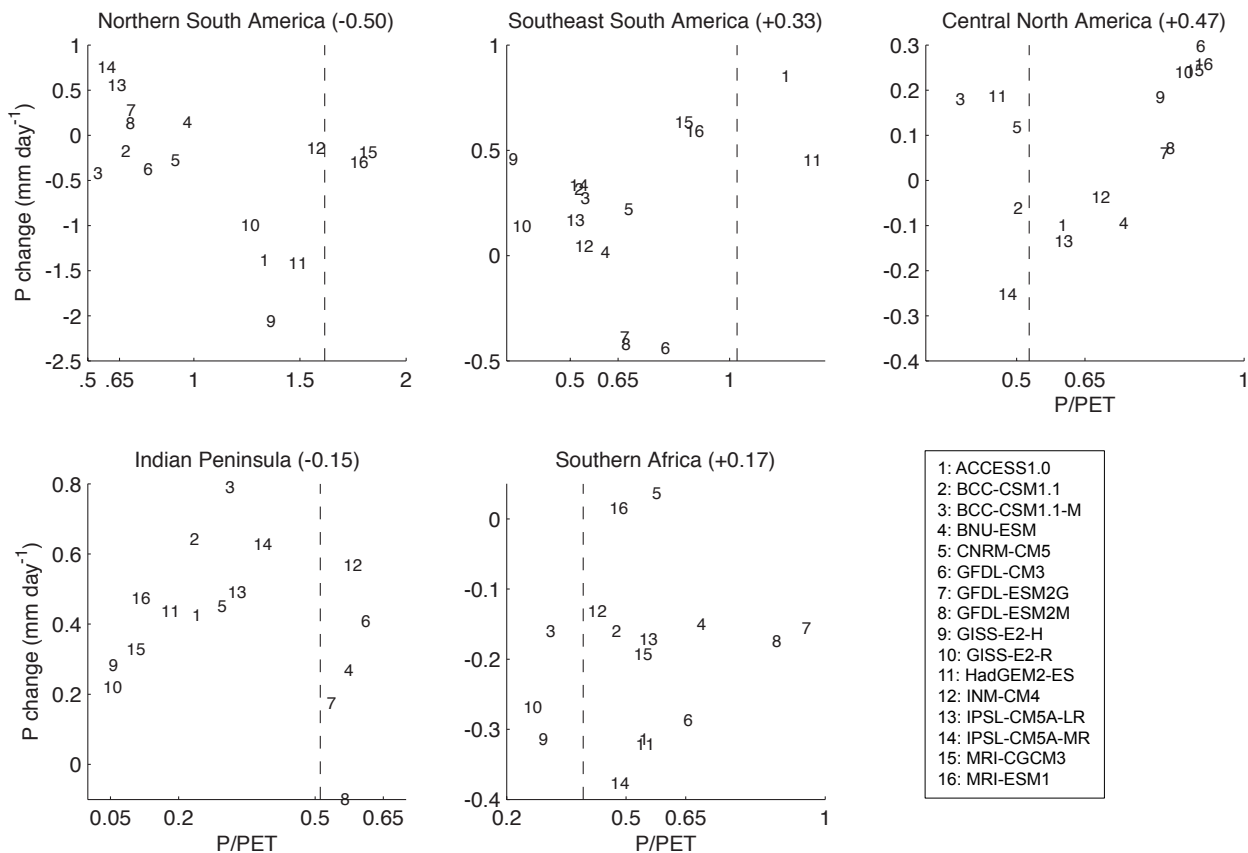


FIG. 7. Regional-land-mean 1981-99 aridity index P/PET vs. 21st-century P change, for each model and region. Values in parentheses are simple correlations of the model points. The dashed line is observational regional-land-mean P/PET . For reference, P/PET less than 0.05 is defined as hyperarid, 0.05 to 0.2 as arid, 0.2 to 0.5 as semiarid, 0.5 to 0.65 as dry subhumid, and more than 0.65 as humid (Middleton and Thomas 1997); see the scale of Fig. 5.

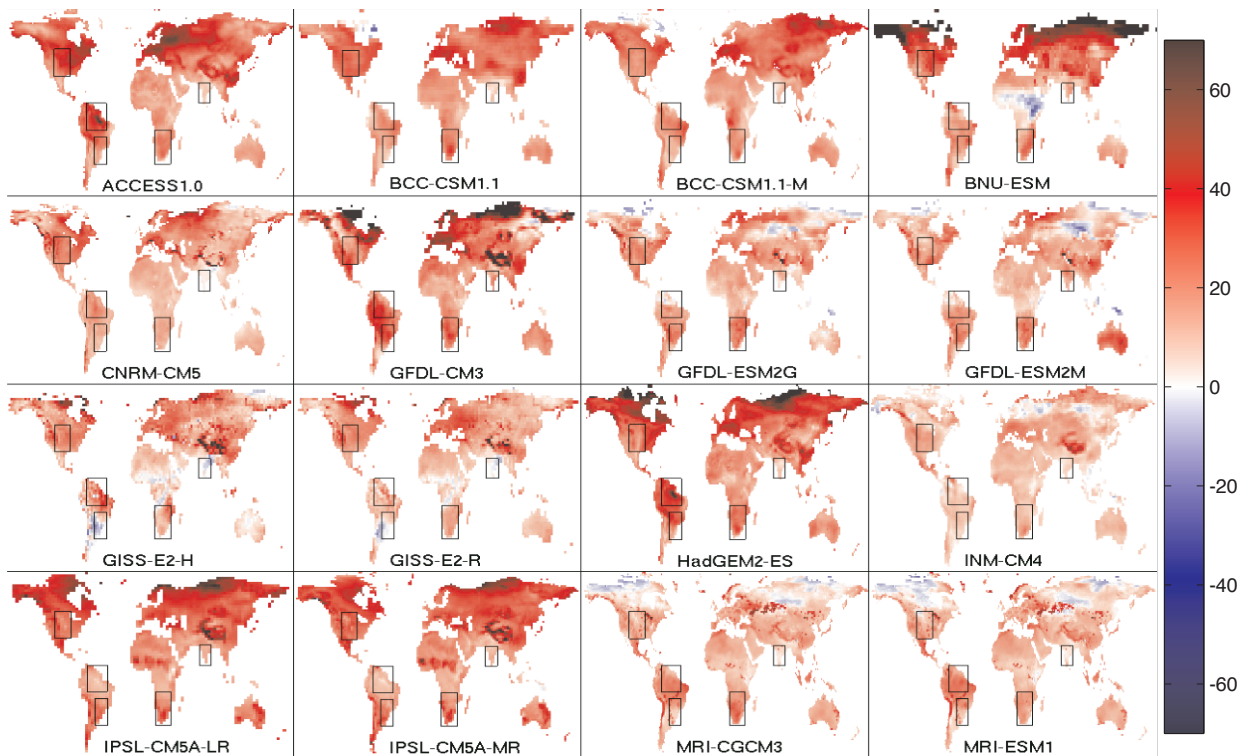


FIG. 8. Percent changes in annual PET between 1981-99 and 2081-99, for each model.

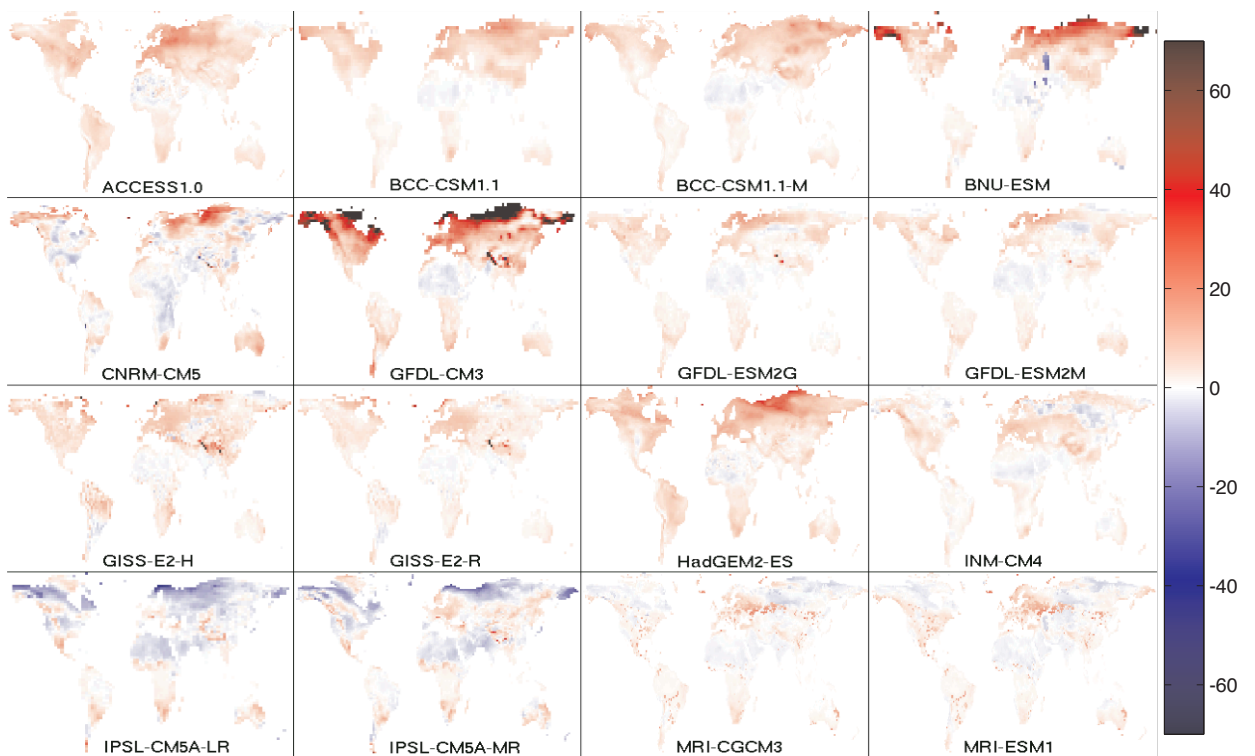


FIG. 9. Differences between the percent changes in annual PET over the 21st century computed using monthly
vs. 3-hourly output.

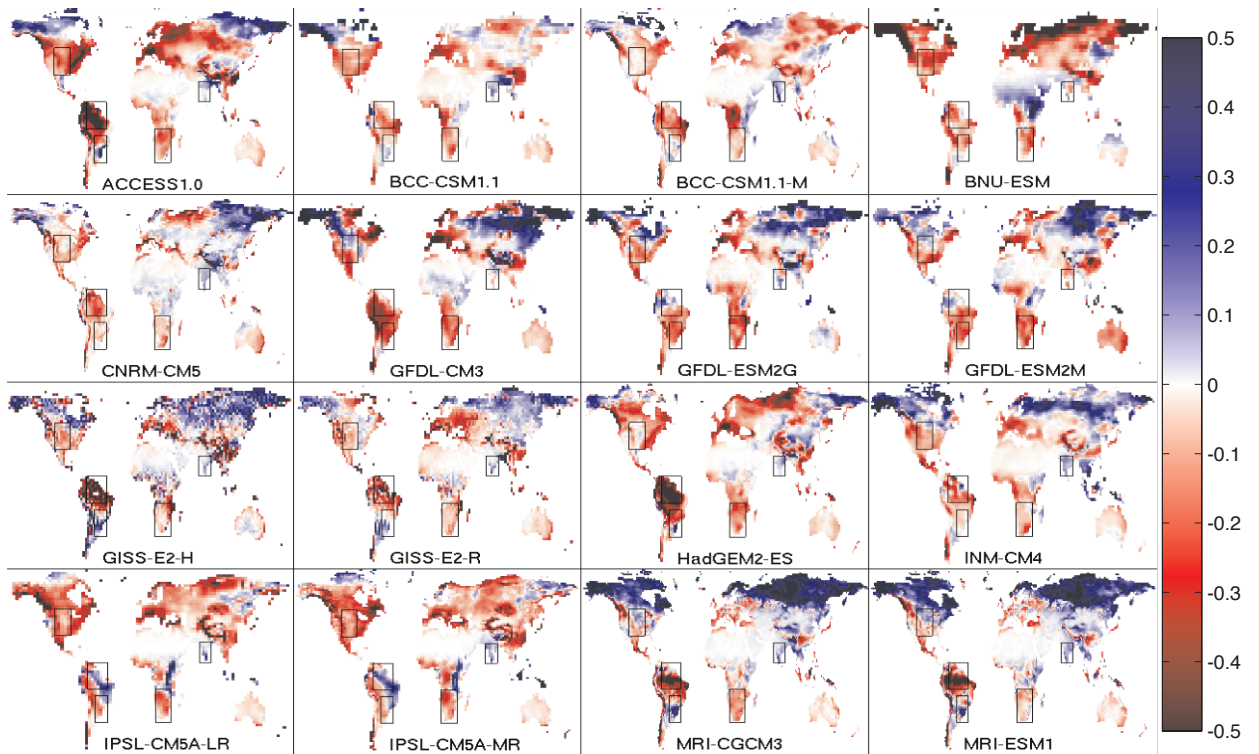


FIG. 10. Changes in the aridity index P/PET between 1981-99 and 2081-99, for each model.

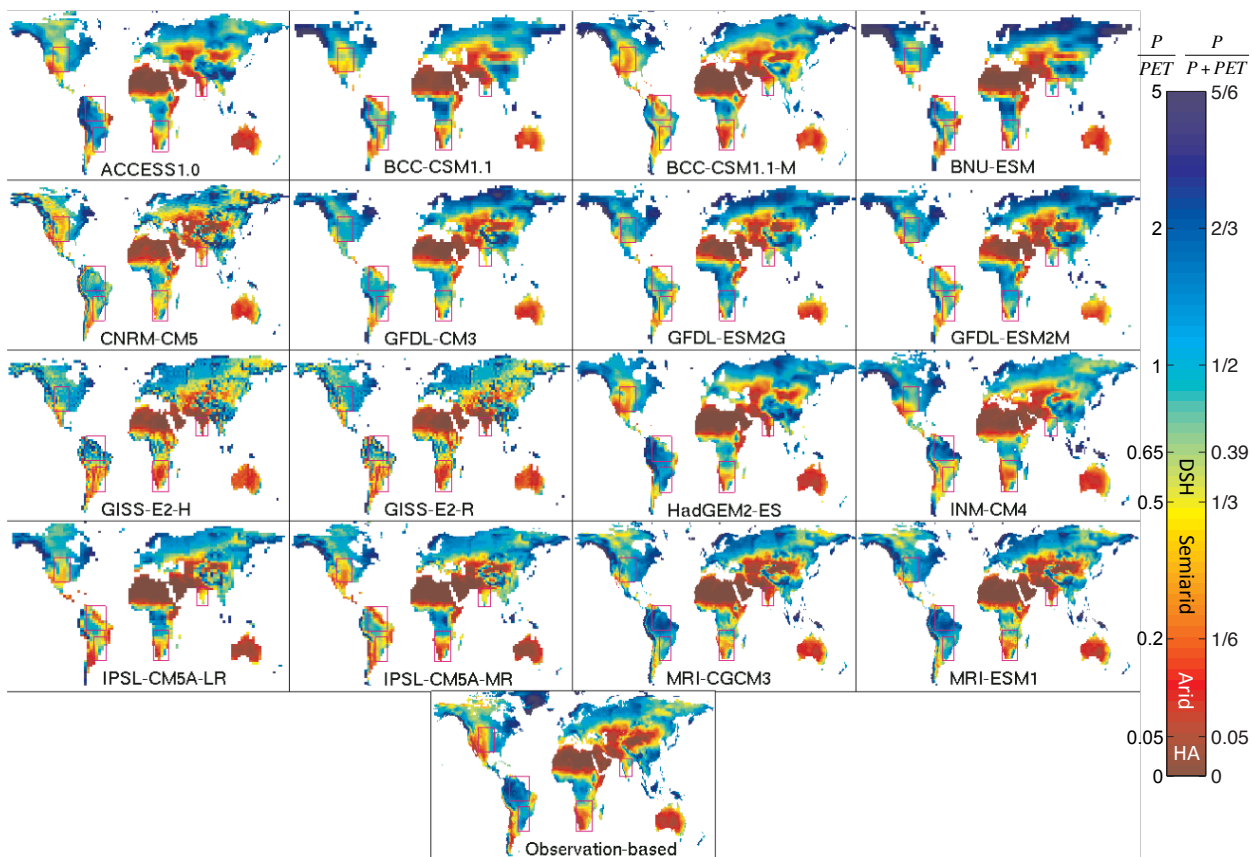


FIG. 11. 1981-99 alternate aridity index $P/(P + PET)$ (right-hand scale) for each model and for the observations. The corresponding P/PET values (left-hand scale) and dryland categories are also shown for reference. Compare to Fig. 5.

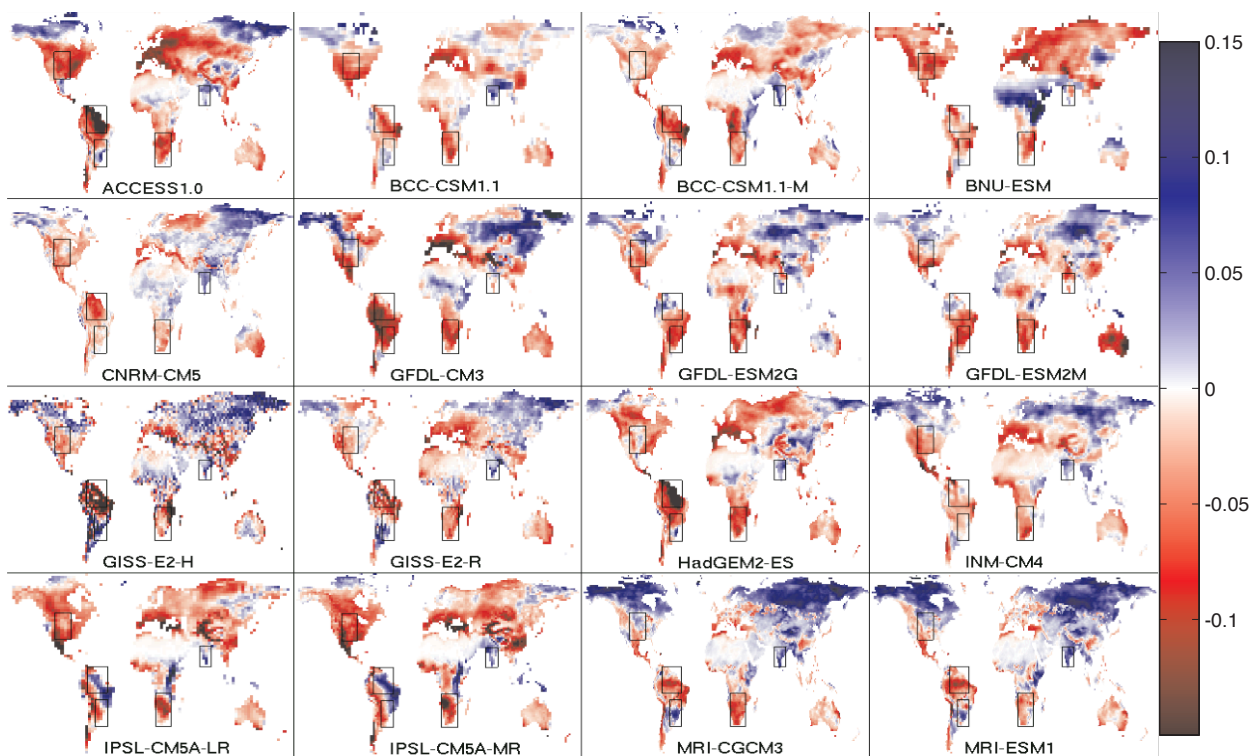


FIG. 12. Changes in the alternate aridity index $P/(P + PET)$ between 1981-99 and 2081-99, for each model.

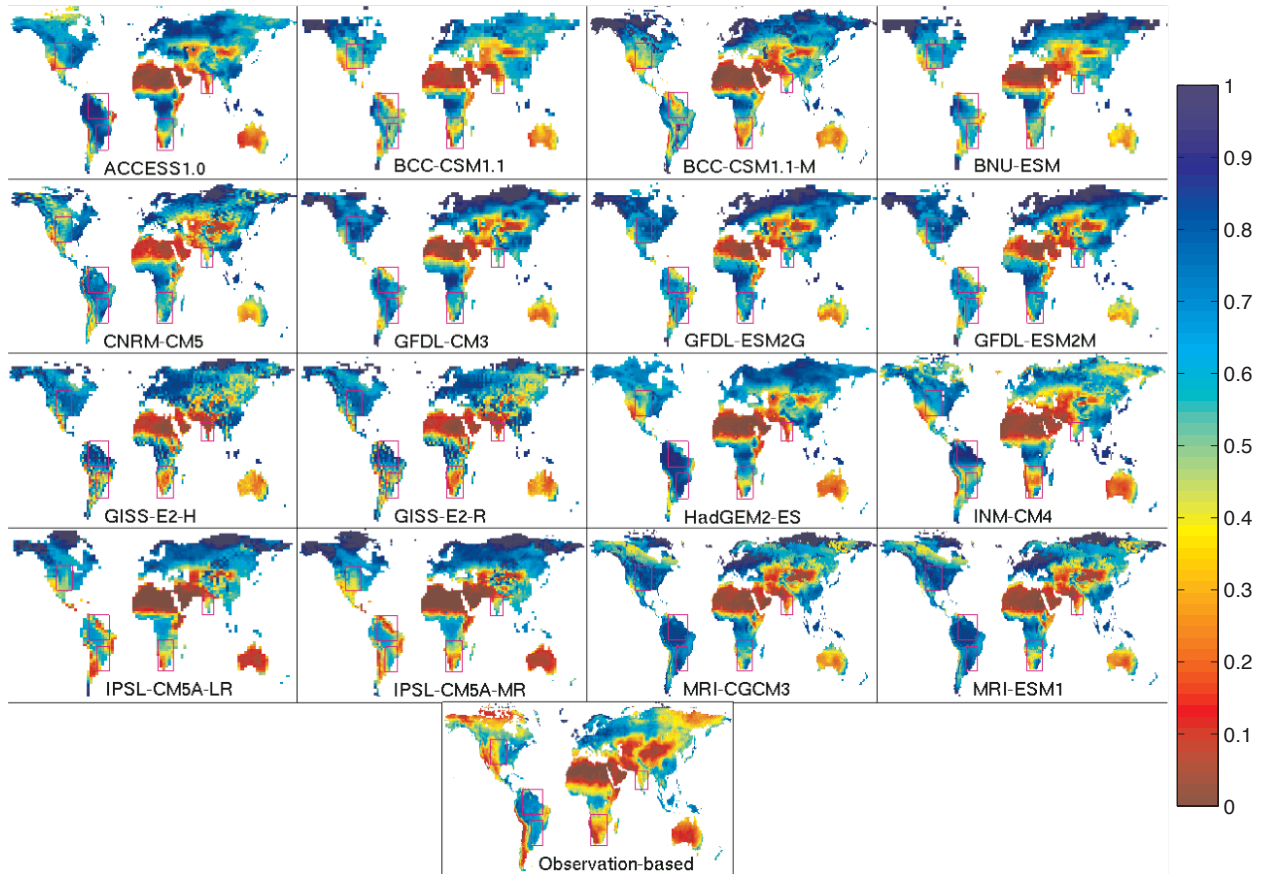


FIG. 13. 1981-99 evaporative fraction $LH/(LH + SH)$ for each model and for the GLDAS observation-driven land model estimate.

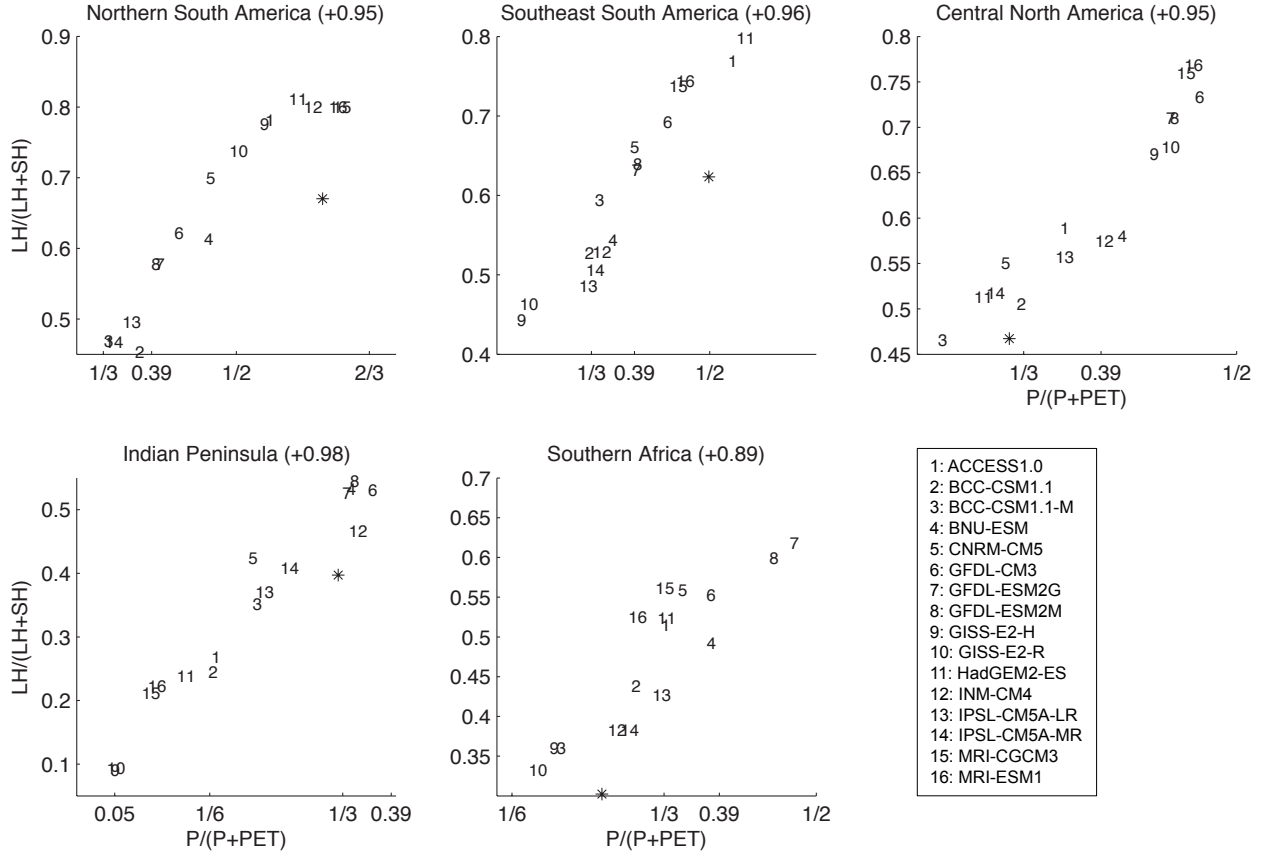


FIG. 14. 1981-99 regional-land-mean alternate aridity index $P/(P+PET)$ vs. evaporative fraction $LH/(LH+SH)$ for each model (numbers) and for the observational products (asterisk), for each region. Values in parentheses are simple correlations of the 16 model points. For reference, $P/(P+PET)$ less than ≈ 0.05 is defined as hyperarid, ≈ 0.05 to $1/6$ as arid, $1/6$ to $1/3$ as semiarid, $1/3$ to ≈ 0.39 as dry subhumid, and more than ≈ 0.39 as humid; see the scale of Fig. 11.

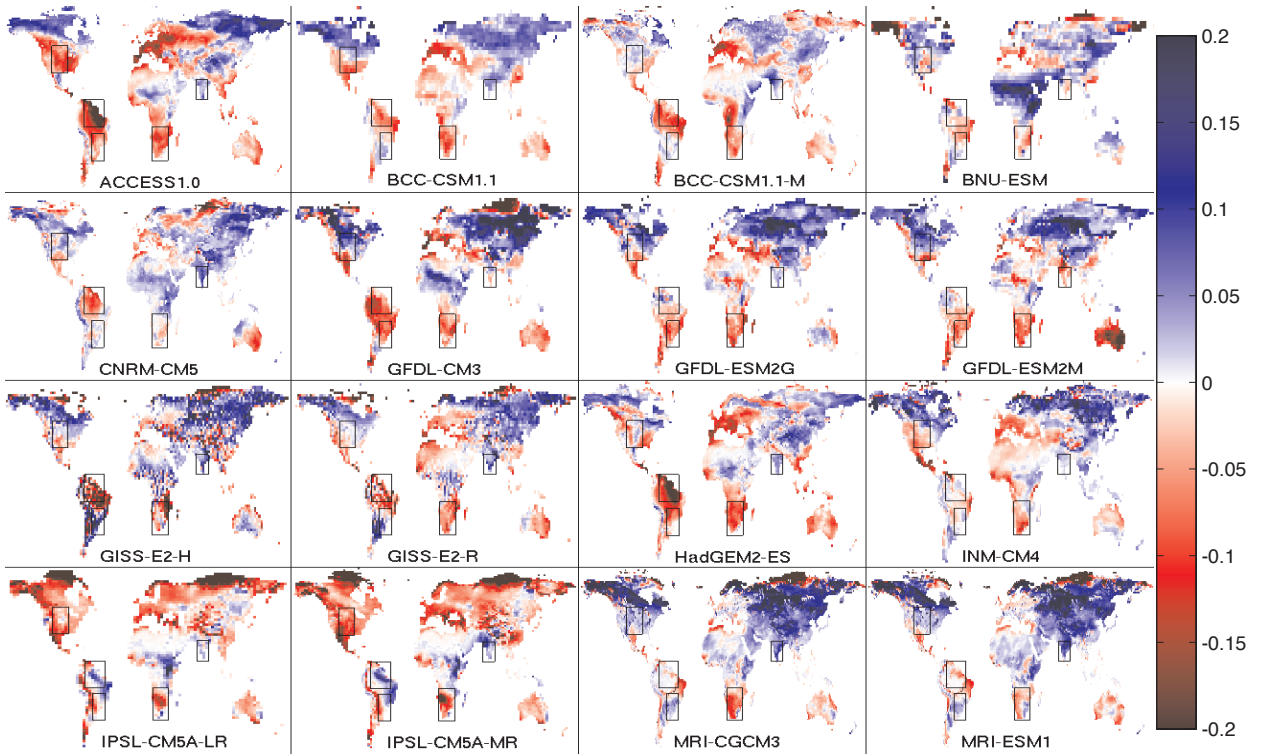


FIG. 15. Changes in evaporative fraction $LH / (LH + SH)$ between 1981-99 and 2081-99, for each model.

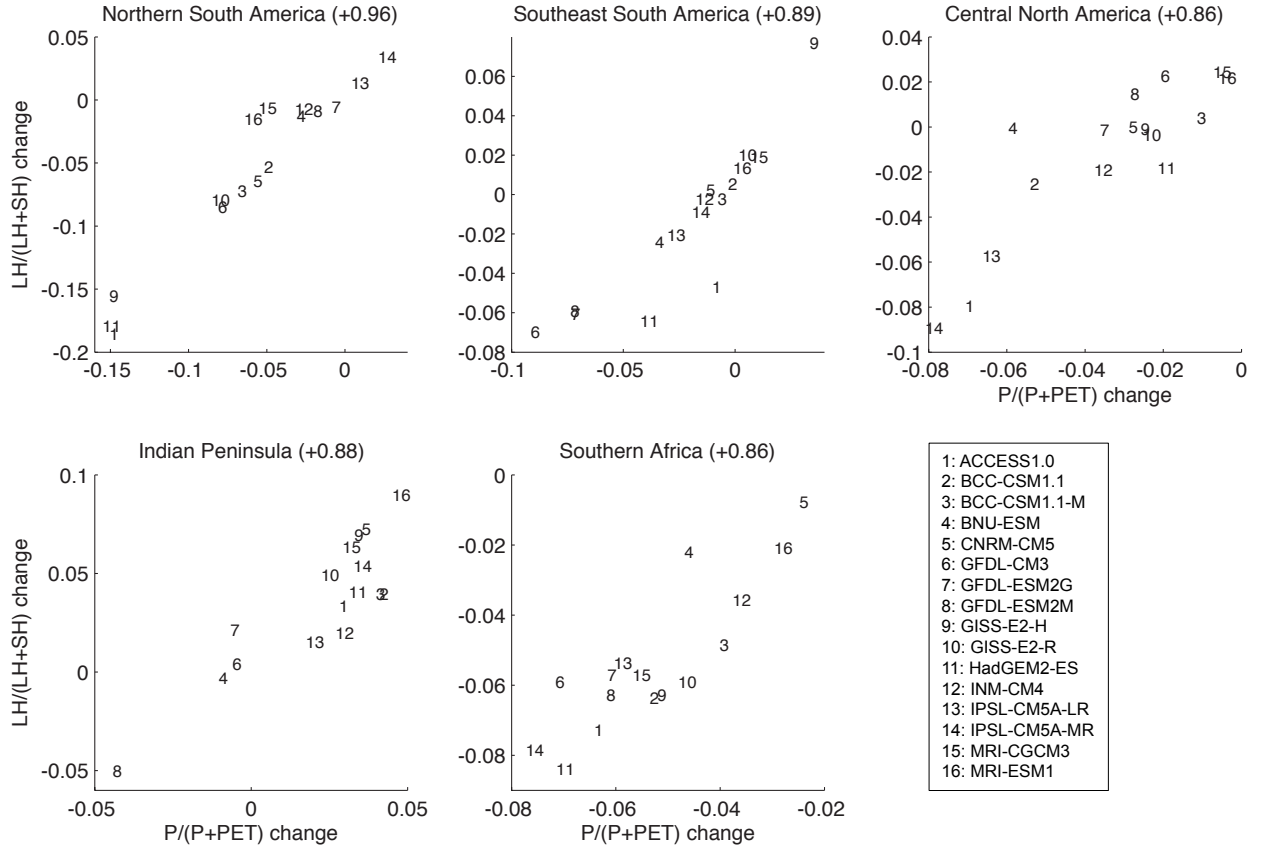


FIG. 16. Regional-land-mean 21st-century $P/(P+PET)$ change vs. $LH/(LH+SH)$ change, for each model and region. Values in parentheses are simple correlations of the model points.